

11-2019

Synchronous Machine Emulation of Vsc for Interconnection of Renewable Energy Sources through HvdC Transmission

Mohamed Asker Kanakkayil

Follow this and additional works at: https://scholarworks.uaeu.ac.ae/electric_theses



Part of the [Engineering Commons](#)

Recommended Citation

Kanakkayil, Mohamed Asker, "Synchronous Machine Emulation of Vsc for Interconnection of Renewable Energy Sources through HvdC Transmission" (2019). *Electrical Engineering Theses*. 5.
https://scholarworks.uaeu.ac.ae/electric_theses/5

This Thesis is brought to you for free and open access by the Electrical Engineering at Scholarworks@UAEU. It has been accepted for inclusion in Electrical Engineering Theses by an authorized administrator of Scholarworks@UAEU. For more information, please contact fadl.musa@uaeu.ac.ae.



جامعة الإمارات العربية المتحدة
United Arab Emirates University

United Arab Emirates University

College of Engineering

Department of Electrical Engineering

SYNCHRONOUS MACHINE EMULATION OF VSC FOR
INTERCONNECTION OF RENEWABLE ENERGY SOURCES
THROUGH HVDC TRANSMISSION

Mohamed Asker Kanakkayil

This thesis is submitted in partial fulfilment of the requirements for the degree of
Master of Science in Electrical Engineering

Under the Supervision of Dr. Hussain Shareef

November 2019

Declaration of Original Work

I, Mohamed Asker Kanakkayil, the undersigned, a graduate student at the United Arab Emirates University (UAEU), and the author of this thesis entitled "*Synchronous Machine Emulation of VSC for Interconnection of Renewable Energy Sources through HVDC Transmission*", hereby, solemnly declare that this thesis is my own original research work that has been done and prepared by me under the supervision of Dr. Hussain Shareef, in the College of Engineering at UAEU. This work has not previously been presented or published or formed the basis for the award of any academic degree, diploma or a similar title at this or any other university. Any materials borrowed from other sources (whether published or unpublished) and relied upon or included in my thesis have been properly cited and acknowledged in accordance with appropriate academic conventions. I further declare that there is no potential conflict of interest with respect to the research, data collection, authorship, presentation and/or publication of this thesis.

Student's Signature: _____



Date: _____

12/02/2020

Approval of the Master Thesis

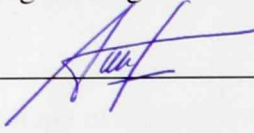
This Master Thesis is approved by the following Examining Committee Members:

- 1) Advisor (Committee Chair): Dr. Hussain Shareef

Title: Associate Professor

Department of Electrical Engineering

College of Engineering

Signature  _____

Date 30/01/2020

- 2) Member: Dr. Addy Wahyudie

Title: Associate Professor

Department of Electrical Engineering

College of Engineering

Signature Addy Wahyudie _____

Date 30/01/2020

- 3) Member (External Examiner): Dr. Hamidreza Zareipour

Title: Professor

Department of Electrical and Computer Engineering

University of Calgary, Canada

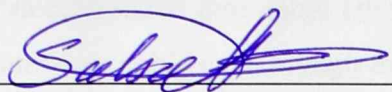
Signature  _____

Date 30/01/2020

This Master Thesis is accepted by:

Dean of the College of Engineering: Professor Sabah Alkass

Signature

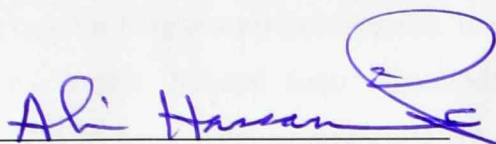


Date

12/2/2020

Dean of the College of Graduate Studies: Professor Ali Al-Marzouqi

Signature



Date

13/2/2020

Copy 1 of 4

Copyright © 2019 Mohamed Asker Kanakkayil
All Rights Reserved

Abstract

The majority of the energy demand over the past years has been fulfilled by centralized generating stations. However, with a continuously increasing energy demand, the integration of decentralized renewable energy sources (RES) into the power system network becomes inevitable even though these sources affect the stability of the grid due to their intermittency and use of various power converters. The transmission of power over long distances from RES is usually accomplished either by AC or DC transmission. High voltage DC transmission (HVDC) is preferred over high voltage AC transmission (HVAC) due to numerous and complex reasons, such as its lower investment cost for long transmission cables, lower losses, controllability, and limited short circuit currents. Several control methods for grid-connected voltage source converters (VSCs), such as power-angle and vector-current controls, are being adopted in RES interconnections. However, these methods face several issues when used for a weak grid interconnection. This thesis develops a control strategy for a VSC–HVDC transmission system by referring to the synchronverter concept. In the proposed method, the sending-end rectifier controls emulate a synchronous motor (SM), whereas the receiving end inverter emulates a synchronous generator (SG) to transmit power from one grid to another. The two converters connected by a DC line provide a synchronverter HVDC (SHVDC) link. Given the high demand for sustainable energy, integrating RES—which can be extended to wind-based resources—into the long-haul HVDC link becomes essential. Therefore, in this thesis, a windfarm with a type 4 permanent magnet SG is integrated into the HVDC link through a rectifier. Depending on the wind speed, the proposed control strategy automatically shares and manages the wind generator power on the DC side by using a battery energy storage system (BESS) connected to the HVDC link to stabilize the power fluctuations generated by the intermittency of the wind farm. The performance of the synchronverter-based HVDC transmission was verified by using a MATLAB Simulink model. Results show that the controller can effectively control the power flow from one grid to another and that the effect of wind fluctuation on the grid can be mitigated by introducing a BESS at the DC link. Therefore, by properly controlling the SHVDC, BESS, and RES connected to the HVDC system, the power from remote RES can be connected to a weak AC grid in a stable manner.

Keywords: Voltage Source Converter (VSC), Synchronverter, High Voltage DC Transmission (HVDC), Renewable Energy Sources (RES), Battery Energy Storage System (BESS).

Title and Abstract (in Arabic)

محاكاة الالات الكهربائية التزامنية لمحول مصدر الجهد (VSC) لربط مصادر الطاقة المتجددة
من خلال خطوط نقل الجهد المستمر عالي الجهد

الملخص

احتلت محطات توليد الطاقة المركزية الجزء الأكبر و الأهم لتلبية الاحتياجات في السابق، و لكن مع تزايد الطلب على الطاقة كان لا بد من دمج المصادر المتجددة للطاقة و تنويع مصادر توليد الطاقة في الشبكة الحالية و توجد العديد من السلبات أو النتائج المترتبة على دمج المصادر المتجددة منها التأثير على ثبات و استقرار الشبكة و الذي بدوره يعود إلى طبيعة هذه المصادر بالإضافة إلى استخدام أنواع مختلفة من محولات الطاقة. تتم عملية نقل الطاقة من مصادر الطاقة المتجددة عبر مسافات طويلة إما عن طريق نقل التيار المتغير أو نقل التيار الثابت، و لكن غالباً يفضل نقل الطاقة عن طريق نقل التيار الثابت ذو الجهد العالي، يعود السبب في ذلك إلى انخفاض التكلفة و الخسائر في الطاقة و حالات انقطاع التيار بالإضافة إلى سهولة السيطرة على هذا النوع من أنواع النقل. يوجد العديد من الطرق المتنبئة للتحكم بمحولات مصادر الجهد المتصلة بالشبكة من أبرزها التحكم عن طريق زاوية الطاقة أو التحكم عن طريق التيار و اتجاهه. بيد أن هناك بعض المشاكل التي يواجهها الناس عند استخدام هذه التقنيات أو الأساليب عند النقاط الضعيفة في الشبكة.

تهدف هذه الأطروحة إلى تطوير استراتيجية للتحكم بمحولات مصادر الجهد المستخدمة في عملية نقل التيار الثابت ذو الجهد العالي بالاعتماد على فكرة التزامن و التحويل. تعتمد هذه الطريقة على وجود طرفان، الطرف المرسل الذي يحتوي على مقوم يقوم بالتحكم عن طريق محاكاة طريقة عمل المحركات المتزامنة، و الطرف المستقبل الذي يقوم بمحاكاة طريقة عمل المولدات المتزامنة. الطرفان متصلان عبر خط تيار ثابت و هذا النوع من الروابط يدعى رابط التزامن و التحويل.

في هذه الأطروحة، ستعمل مزرعة الرياح التي تتكون من النوع الرابع من المولدات المتزامنة التي تحتوي على مغناطيسات دائمة باستخدام رابط التزامن و التحويل عن طريق المقوم معاً. اعتماداً على سرعة الرياح سوف تتم مشاركة و إدارة استراتيجية التحكم بالطاقة بمولدات الرياح من طرف التيار الثابت بشكل تلقائي، بالإضافة إلى ذلك يوجد نظام مكون من بطاريات لحفظ الطاقة متصلة برابط التزامن و التحويل و ذلك بهدف المحافظة على استقرار التقلبات في الطاقة

بسبب طبيعة الرياح الغير مستقرة. تم إثبات فعالية هذا النظام المتكامل عن طريق استخدام برنامج المات لاب للمحاكاة، و أكدت النتائج على أن هذا النوع من الأنظمة يمكنه التحكم بشكل فعال باتجاه و تدفق الطاقة من شبكة إلى أخرى. و تؤكد النتائج أيضاً أنه من الممكن تقليل تأثير الرياح و طبيعتها الغير مستقرة عن طريق نظام البطاريات المستخدمة لحفظ الطاقة و المتصلة بالرابط. في الختام، يمكننا القول بأن هذا النوع من الأنظمة المتكاملة يساعد في عملية ربط الطاقة عن بعد من مصادر الطاقة المتجددة بالنقاط الضعيفة في الشبكة بطريقة ثابتة و مستقرة.

مفاهيم البحث الرئيسية: المحول مصدر الجهد ، التيار المستمر عالي الجهد ، مصادر الطاقة المتجدده ، نظام البطاريات لتخزين الطاقه ، محول متزامن.

Acknowledgements

This thesis turns into a reality with the caring and help of numerous people and I might want to stretch out my earnest gratitude to every one of them.

Foremost, I want to offer my special thanks and gratitude to my advisor Dr. Hussain Shareef for guiding all through the work and supporting to enhance the knowledge and skill for this study.

I would like to say thanks to Dr. Mousa Hussain for his consistent help and support which helped me to finish this thesis. I also thank my fellow mates Mr. Fasal Rahman, Mr. Nakul Narayanan for the continuous motivation and immense support.

Last but not the least, I would like to thank My spouse Ms. Vaseela, my son Fezin Haadi and my parents for their continuous support during my study at UAEU.

Dedication

To my beloved parents and family

Table of Contents

Title	i
Declaration of Original Work	ii
Copyright	iii
Approval of the Master Thesis	iv
Abstract	vi
Title and Abstract (in Arabic)	viii
Acknowledgements	x
Dedication	xi
Table of Contents	xii
List of tables	xv
List of Figures	xvi
List of Abbreviations.....	xviii
Chapter 1: Introduction	1
1.1 Overview	1
1.2 Basics of HVDC.....	1
1.3 HVDC System Configurations.....	3
1.3.1 Monopolar HVDC Link	3
1.3.2 Bipolar HVDC Link	4
1.3.3 Homopolar Link	4
1.3.4 Back-to-Back HVDC System.....	5
1.4 Conventional HVDC Transmission and VSC-HVDC Transmission	5
1.5 VSC-HVDC Link Structure	7
1.6 Wind Turbine Configurations	8
1.6.1 Power Contained in Wind.....	8
1.6.2 Wind Turbine Ratings and Specifications	9
1.6.3 Types of Wind Turbines	9
1.7 HVDC Transmission Control Methods.....	13
1.7.1 Power Angle Control.....	14
1.7.2 Vector Control	15

1.7.3 Power Synchronization Control.....	22
1.8 DC Link Capacitor	25
1.9 Synchronverter	26
1.10 Renewable Energy Integration.....	27
1.11 Problem Statement	28
1.12 Objective	29
1.13 Scope of Work	29
1.14 Summary	30
Chapter 2: Modelling and Control Techniques	32
2.1 Modeling of Synchronous Machines	32
2.2 VSC-HVDC Transmission System Configurations.....	36
2.3 Synchronverter-Based HVDC Control	37
2.3.1 Synchronverter	38
2.3.2 Synchronverter Implementation	39
2.4 Battery Energy Storage System Control	42
2.5 Phase Locked Loop.....	43
2.6 Boost Converter	44
2.7 Summary	45
Chapter 3: Extension of the Synchronverter Concept for the Auto Regulation of Power Flow Between Two Grids.	46
3.1 Power Flow Control between Two Grids by Using a Synchronverter	48
3.2 Integration of Type 4 Wind Farm into the HVDC Link	52
3.3 Integration of Wind Farm Between Two Grids and the Auto Regulation of Power Flow Between Two Grids	53
3.4 HVDC Power Stabilization using BESS.....	55
Chapter 4: Results and Discussion.....	56
4.1 Phase Locked Loop.....	56
4.2 Case 1: Power Flow between Two Grids Measured by a Synchronverter	56
4.3 Case 2: Real Power Graph for the Synchronous Machine Emulation of VSC-HVDC Transmission Interconnected with Wind Farm	58

4.4 Case 3: Real Power Graph for the Synchronous Machine Emulation of VSC-HVDC Transmission Interconnected with a Wind farm and BESS.	60
Chapter 5: Conclusion.....	63
References	64

List of Tables

Table 1: System parameters and its values.	46
---	----

List of Figures

Figure 1: Monopolar HVDC link.....	3
Figure 2: Bipolar HVDC link.....	4
Figure 3: Homopolar link.....	5
Figure 4: Back-to-Back HVDC System.....	5
Figure 5: HVDC Technology based on CSC.....	6
Figure 6: VSC-HVDC Technology.....	6
Figure 7: VSC-HVDC Link Structure.....	7
Figure 8: Fixed Speed Wind Turbine.....	10
Figure 9: Variable Slip Wind Turbine.....	11
Figure 10: Double Fed Induction Generator Wind Turbine.....	12
Figure 11: VSC Conventional Vector Control Approach.....	18
Figure 12: Conventional Vector Control Method for HVDC Transmission.....	20
Figure 13: Control and Structure of the VSC-HVDC System.....	21
Figure 14: Synchronization Mechanism Between Two Synchronous Machines in AC System.....	23
Figure 15: Phasor Diagram Synchronization (Steady State).....	24
Figure 16: Phasor Diagram Synchronization (Phase Shifting of an Equivalent Inner EMF).....	24
Figure 17: Structure of idealized three phase round rotor SG.....	33
Figure 18: VSC Structure.....	37
Figure 19: Synchronverter Based HVDC Transmission.....	39
Figure 20: Power part of Synchronverter.....	40
Figure 21: Electronic Part of a Synchronverter.....	42
Figure 22: PLL Block Diagram.....	44
Figure 23: Boost Converter.....	44
Figure 24: Synchronous Machine Emulation of VSC-HVDC Transmission System.....	47
Figure 25: MATLAB Model of the Synchronverter Control for the Constant Power Mode End.....	50
Figure 26: MATLAB Model of the Synchronverter Control for the Constant Voltage Mode End.....	51
Figure 27: MATLAB Model of a Type 4 Wind Farm.....	52
Figure 28: Synchronous Machine Emulation of VSC for the Interconnection of Wind farm Through HVDC Transmission.....	54
Figure 29: BESS System.....	55
Figure 30: PLL curve.....	56
Figure 31: Real Power Graph for Synchronous Machine Emulation of VSC-HVDC.....	57
Figure 32: DC Link Voltage Graph at Both Converter Stations.....	58

Figure 33: Real Power Graph for the Synchronous Machine Emulation of VSC-HVDC Transmission Interconnected with a Wind Farm.....	58
Figure 34: DC link Voltage Graph for the Synchronous Machine Emulation of VSC-HVDC Transmission Interconnected with a Wind Farm.....	59
Figure 35: Close view of DC Voltage Curve at Steady State	59
Figure 36: Real Power Graph for Synchronous Machine Emulation of VSC-HVDC Transmission Interconnected with a Wind Farm and BESS.	60
Figure 37: DC Link Voltage Curve for the Synchronous Machine Emulation of VSC-HVDC Transmission Interconnected with a Wind farm and BESS.	61
Figure 38: Grid Power Graph with BESS	61
Figure 39: Grid Power Curve without BESS	62

List of Abbreviations

AC	Alternating Current
BESS	Battery Energy Storage System
CSC	Current Source Converter
DC	Direct Current
DSP	Digital Signal Processor
EMF	Electromotive Force
HVAC	High Voltage Alternating Current
HVDC	High Voltage Direct Current
IGBT	Insulated Gate Bipolar Transistor
LCC	Line Commutated Converter
PLL	Phase Locked Loop
PMA	Permanent Magnet Alternator
PMSG	Permanent Magnet Synchronous Generator
PWM	Pulse Width Modulation
RES	Renewable Energy Source
SG	Synchronous Generator
SHVDC	Synchronous High Voltage DC Transmission
SM	Synchronous Machine
VCO	Voltage Controlled Oscillator
VSC	Voltage Source Converter
WECS	Wind Energy Conversion System
WEG	Wind Energy Generator

Chapter 1: Introduction

1.1 Overview

The practical use of high voltage DC (HVDC) transmission technologies for long range transmission has been proven in the past. However, the ongoing technological revolution demands more energy for advancement and growth, thereby highlighting the importance of effectively handling electrical energy. A developing world demands an efficient generation and transmission of electrical power, and part of this demand is met by effectively handling and generating electrical power from growing distributed energy sources. Therefore, the use of HVDC transmission technology and the integration of distributed electric generation into HVDC transmission links have become inevitable.

HVDC transmission is an effective method for transmitting large amounts of power over a long distance. This method has become popular worldwide due to the advancements in power electronics technologies.

The first HVDC transmission in the world took place in 1954 when the island of Gotland (Sweden) was connected to Sweden through undersea cables. Thyristor with 50 KV and 100 A were used for the transmission.

1.2 Basics of HVDC

An HVDC link equipped with rectifiers or inverters is connected to AC grids. These rectifiers and inverters convert the alternating AC voltage into a constant DC voltage and back to alternating AC voltage. The HVDC links demonstrate several advantages over HVAC, some of which are listed below (Saksvik, 2012):

1. Lower transmission losses over long distances.

2. Enabling high-power transmission over a long distance by using underground cables.
3. Enabling the connection of asynchronous grids.
4. An efficient control of power flow, which enables power trading among different regions.
5. Smaller footprint compared with overhead AC transmission lines.
6. Capability of using submarine cables over a long distance to transmit a large amount of power.
7. Better grid stability with full control of power flow and good response under transient conditions in AC grids.
8. Significantly less magnetic fields compared with AC lines.
9. Fast recovery from power failures by using nearby grids.

However, due to the cost of HVDC converter stations, HVDC is more expensive than high voltage AC (HVAC) transmission. Nevertheless, this cost is only a one-time cost, and HVAC is too expensive to operate due to its unacceptable transmission losses and the nature and location of most renewable energy sources (RES). In addition, HVDC has a smaller footprint compared with HVAC, thereby making the former highly suitable for long distance transmission using long underground or submarine cables.

HVDC has many applications in the power industry. For instance, this technology facilitates a long-distance bulk power transmission, which is essential for hydropower resources, which are mainly located in remote areas, thereby making the bulk transmission of power to load centers inevitable. HVAC transmission is a conventional method of transmitting power that demands a greater number of lines, reactive power compensation, and wider right of ways. Therefore, in such cases, using LCC-HVDC

technology is necessary for the economy and profitability. HVDC also shows much flexibility in interconnecting two asynchronous grids by using back-to-back converters and in enabling underground or submarine cable transmissions. This technology can also improve the stability of the grid by promoting stabilized and controlled power flows. The offshore transmission of power generally originates from wind farms. The VSC transmission system provides some flexibility to isolate the wind farm from the grid, and a VSC-HVDC transmission network can compensate reactive power to wind farms and to the interconnection point.

1.3 HVDC System Configurations

The HVDC system can be configured in several ways. The choice of HVDC system configurations depends on the function and location of the converter station.

1.3.1 Monopolar HVDC Link

A monopolar HVDC link comprises a single conductor of negative polarity, and the return path of current is acted by earth or sea. Metallic return is also used in some cases. Two converters are placed at the end poles to convert AC to DC and vice versa as shown in Figure 1.

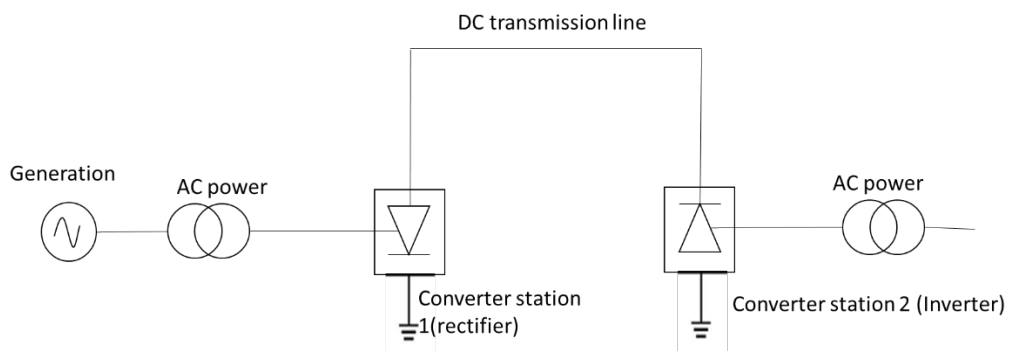


Figure 1: Monopolar HVDC link

1.3.2 Bipolar HVDC Link

A bipolar link comprises two conductors, one of which is positive and the other negative. The converters are placed at both end poles. Earthing is implemented at the midpoint of the converter stations through electrodes. The voltage of these electrodes is half of the conductor voltage placed for transmission. The system can also operate as a monopolar link by using the ground returning technique when any of the two links do not operate. The system structure is shown in Figure 2.

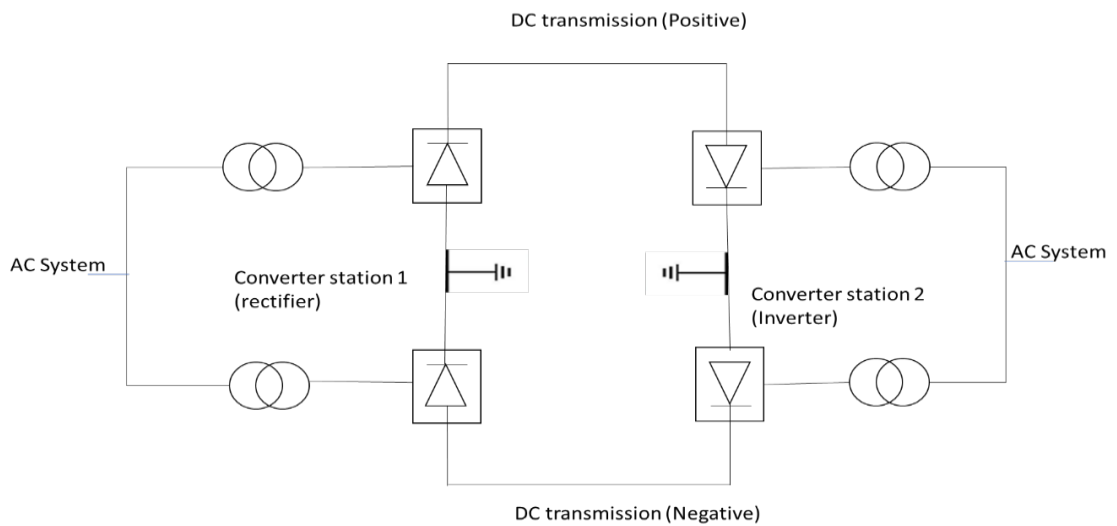


Figure 2: Bipolar HVDC link

1.3.3 Homopolar Link

The homopolar link comprises two conductors with the same polarity (typically negative) and a return path by earth or metallic. The poles are operated in parallel to reduce insulation expenses. The system structure is shown in Figure 3.

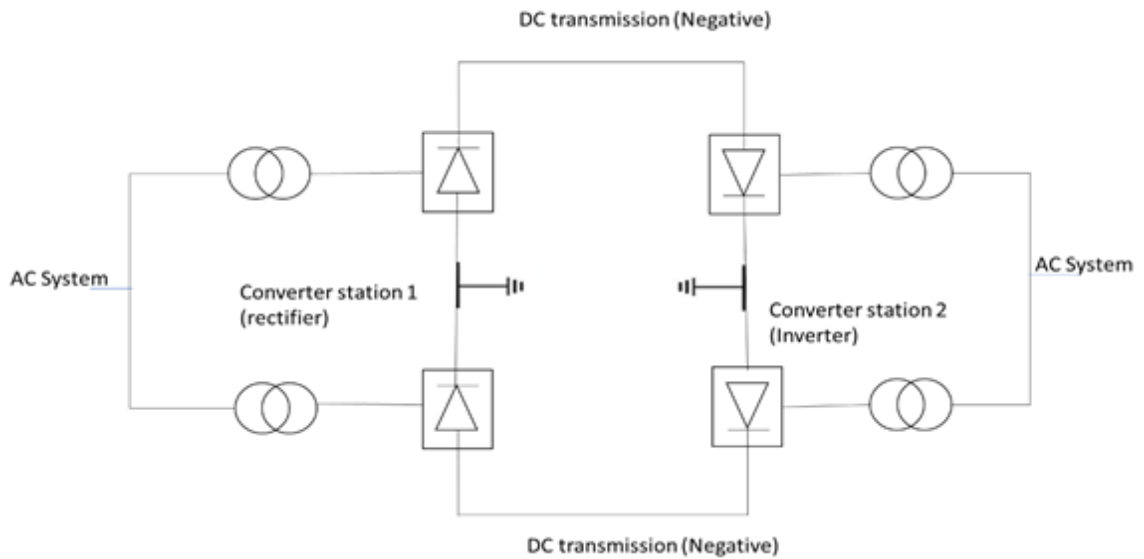


Figure 3: Homopolar link

1.3.4 Back-to-Back HVDC System

A back-to-back system uses two converter stations at the same site and does not transmit power over the DC line. This system is mainly used to interconnect two asynchronous systems. The structure of a typical back-to-back system is shown in Figure 4.

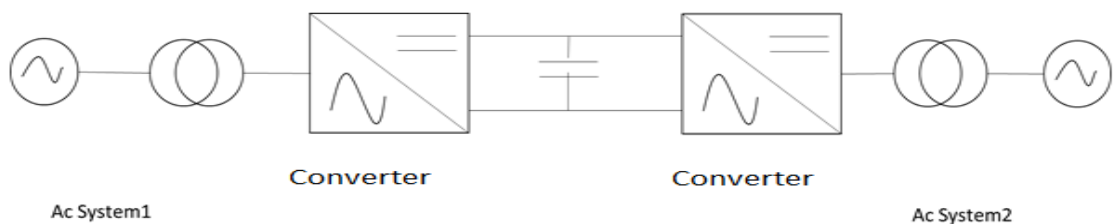


Figure 4: Back-to-Back HVDC System

1.4 Conventional HVDC Transmission and VSC-HVDC Transmission

HVDC transmission can be realized by using current source converters (CSCs), commutated thyristor switches (traditional or classic HVDC), or voltage source converters (VSC-HVDC).

The current source converter was introduced in the 1950s as the first HVDC conventional technology. HVDC is operated with thyristor switches and controls the direction of the active power flow with the DC voltage polarity (Hingorani & Gyugyi, 1999). Figure 5 shows the structure of CSC-based HVDC technology.

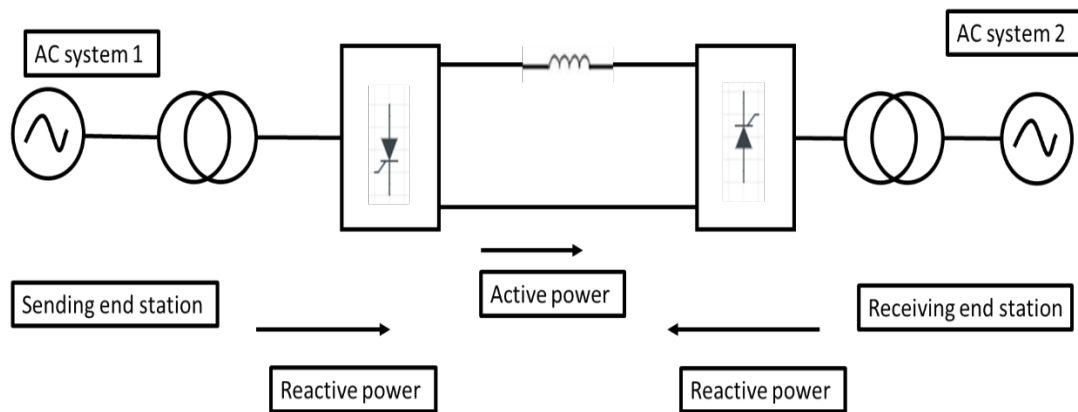


Figure 5: HVDC Technology based on CSC

Given the advancements in power electronic devices with the switch off ability and in DSPs that can generate suitable firing patterns, VSCs have become highly suitable for HVDC transmission applications. The first IGBT switches for HVDC were implemented in Australia for a 180 MW, 80 kV, and 59 km line (De Andrade & De Leao, 2012). This technology can reverse the direction of the power flow by reversing the DC current without reversing the DC voltage polarity (Hingorani & Gyugyi, 1999). Figure 6 shows the structure of the VSC-HVDC technology.

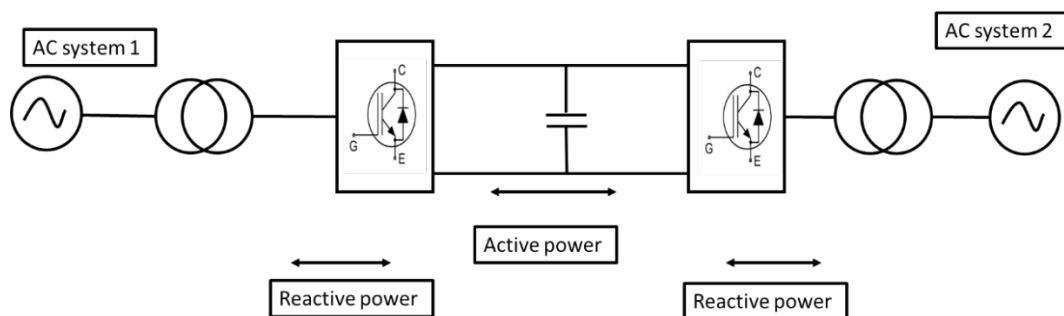


Figure 6: VSC-HVDC Technology

VSCs generally use IGBT and pulse width modulation (PWM) to produce the desired shape of the waveform. VSC-HVDC is more flexible and intelligent than CSC-HVDC and has a better adaptability to the transmission of power from variable power sources, such as wind farms.

The main advantage of VSC-HVDC over CSC-HVDC lies in its high controllability. Meanwhile, CSC-HVDC has a very high capacity for transmitting power over long distances. Both VSC and CSC follow the same theory of HVDC and use the same auxiliary subsystems. Therefore, both of these systems can compete with HVAC in terms of transmitting power over long distances.

1.5 VSC-HVDC Link Structure

A VSC-HVDC link structure has three major parts, namely, the DC and AC circuits and the VSCs. Figure 7 illustrates the VSC-HVDC link structure (Imhof, 2015).

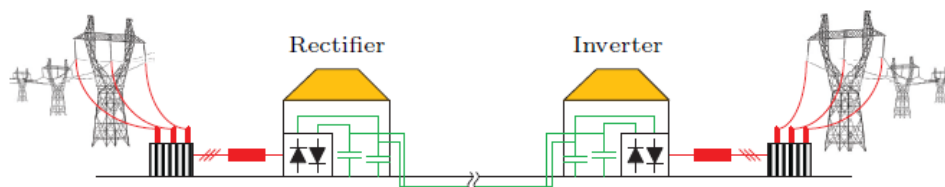


Figure 7: VSC-HVDC Link Structure

A step-down transformer brings the three-phase AC voltage from the grid down to a desired level for the VSC. The three-phase reactor then drives the AC current to provide a current source characteristic on the AC side. The VSC includes a rectifier and an inverter, of which the former converts AC into DC, whereas the latter does the opposite. Each converter has two control degrees. The rectifier controls the active

power at the DC link of the converter and the reactive power at the AC side, whereas the inverter controls the reactive power at the AC side and the voltage at the DC side of the converter. Large capacitors are installed at the DC side of converters to ensure that the DC side acts as a voltage source. The VSC in transmission lines provides some degree of freedom to control the active and reactive power at the terminals of the VSC-HVDC link. Therefore, VSCs are not only used for power transmission but also for power system control.

1.6 Wind Turbine Configurations

Wind energy or wind power describes how the kinetic energy of wind is utilized to generate mechanical power or electricity. Wind power systems have been used for water pumps and windmills and have been later used to convert mechanical energy into electrical energy. With the increasing global demand for renewable energy, electrical engineers have studied how windmills can be used to generate electrical energy.

1.6.1 Power Contained in Wind

The power contained in wind is computed as follows by the kinetic energy of the flowing air mass per unit time:

$$P_o = \frac{1}{2} (\text{air mass per unit time}) (\text{wind velocity})^2$$

$$P_o = \frac{1}{2} (\rho A V_\infty) (V_\infty)^2$$

$$P_o = \frac{1}{2} \rho A V_\infty^3 \quad (1.1)$$

where P_O is the power contained in wind (watts), ρ is the air density, A is the rotor area (m^2), and V_∞ is the wind velocity without rotor interference (ideally at infinite distance from the rotor).

1.6.2 Wind Turbine Ratings and Specifications

Given that a wind turbine varies its electrical power output depending on the wind speed, a standard procedure for determining the rating of a machine must be established. Some manufacturing companies mention the power rating along with wind speed at which the previously mentioned power rating is achieved. This method is highly favorable for manufacturers given the absence of any clear-cut method for defining wind speed, which is being kept being on the higher side which in turns reflects a higher power rating.

Combining rotor diameter with the peak power rating of a generator can provide a very meaningful method for determining the rating of a machine. Specific rated capacity (SRC) is an index used for comparing different wind turbine designs and is defined as the ratio of the power rating of the generator to the rotor swept area. The SRC for small to large rotors varies between 0.2 and 0.6.

1.6.3 Types of Wind Turbines

Wind turbines are generally classified into four categories.

1.6.3.1 Fixed Speed-Wind Turbines (Type 1)

Fixed-speed wind turbines are the most basic types of utility-scale wind turbines that operate at fixed speeds (i.e., approximately less than 1% variation in rotor speed). Squirrel cage induction machines are used for these turbines and are directly connected to the grid. The power generated from wind is typically controlled by using pitch

controllers. In some cases, fixed-speed wind turbines are also equipped with stall controllers. In pitch-controlled turbines, the blades can turn a few degrees to align with the wind, whereas in stall-controlled turbines, the blades are rigidly fixed to the hub, thereby changing the laminar flow into turbulent flow at high-speed winds, resisting the mechanical power extracted from wind, and protecting the induction machine from overload. However, as a major drawback, the energy absorbed from wind by using stall-controlled turbines is suboptimal.

Nevertheless, fixed-speed wind turbines are inexpensive, easy to maintain, and widely used in the field. These turbines generally consist of a turbine rotor and blade assembly, shaft and gearbox unit, induction generator, and a control system as shown in Figure 8.

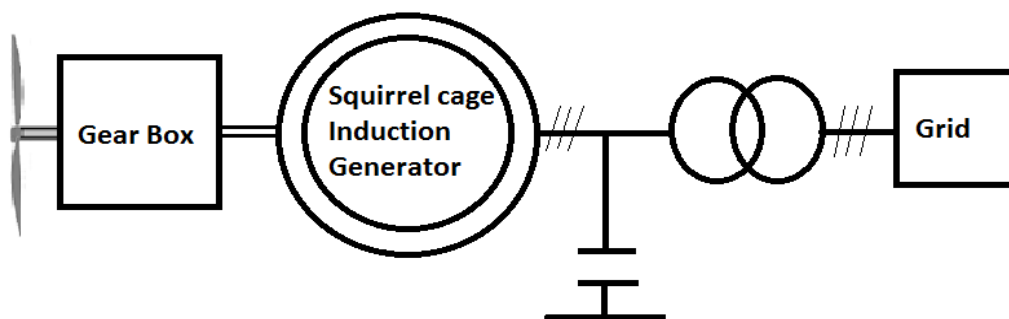


Figure 8: Fixed Speed Wind Turbine

1.6.3.2 Variable-Slip Wind Turbine Generator (Type 2)

Despite their many benefits, including their robustness, simplicity, and low cost, fixed-speed wind turbines cannot optimally capture power from wind. Variable-slip wind turbines are installed to address this problem. These wind turbines rely on rotor resistance control to establish power control. Unlike fixed-speed wind turbines,

variable-slip wind turbines use a wound rotor machine with connected external resistance instead of a squirrel cage machine. The structure of a typical variable-slip wind turbine is shown in Figure 9.

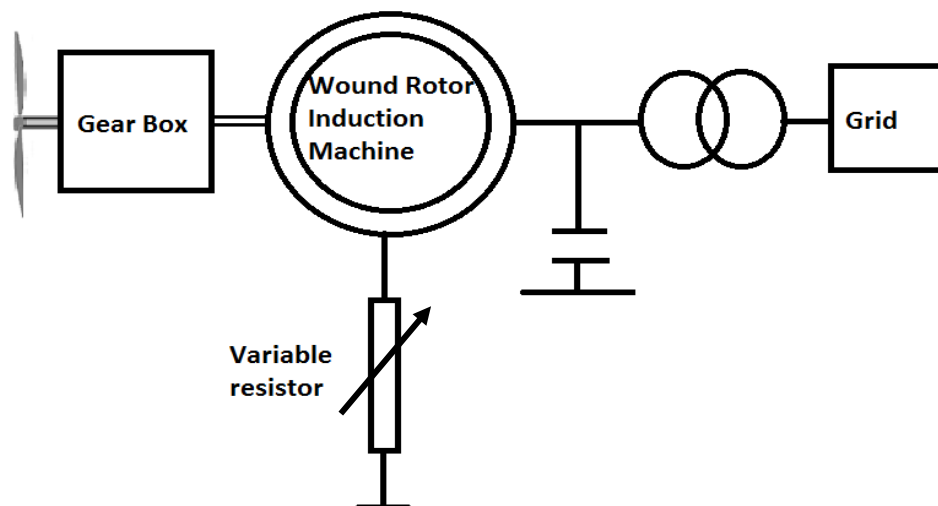


Figure 9: Variable Slip Wind Turbine

1.6.3.3 Double-Fed Induction Generator (DFIG) Wind Power Plant (Type 3)

In a DFIG system, the maximum amount of energy is captured by using a power electronic interface that controls the rotor current to establish variable speed under variable winds. The power electronics interface units process the rotor power, which is usually less than 25% of the total output power. In this way, the speed is controlled at low cost and minimal power loss.

DFIG operates as a wound rotor induction generator with integrated power electronic circuits on its rotor and stator windings to optimize the operation of wind turbines. These circuits can capture power from the wind better than squirrel cage induction generators. The turbines being developed nowadays have a larger diameter due to the advancements in these technologies, which demand longer blades rotating at lower angular speeds and at acceptable noise levels. In this way, DFIG can control speed at

low cost and minimal power loss. Gear boxes are also used to increase the angular speed of the induction generator.

Wound rotor induction machines are used in DFIG wind turbines. Rotor circuits are accessed by using slip rings and brushes, and a three-phase supply is fed to the stator winding that is generally less than 1 kV at a frequency of 50 Hz–60 Hz. Rotor excitation is achieved by a back-to-back AC–DC–AC converter that is used to rectify and convert the supply voltage into the required three-phase AC with a desired frequency. The slip power is processed by a power converter connected to the rotor winding. Therefore, independent excitations are provided for the stator and rotor windings of a DFIG.

The methods for controlling real and reactive power are either established by a vector control or field oriented through direct torque control. Figure 10 illustrates the structure of a DFIG wind turbine.

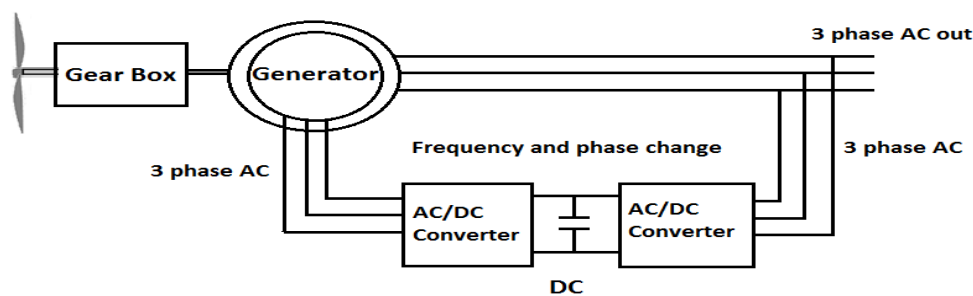


Figure 10: Double Fed Induction Generator Wind Turbine

1.6.3.4 Full Converter Wind Turbines (FCWT; Type 4)

An FCWT is equipped with a permanent magnet rotor and shows several advantages over other wind turbines. For instance, an FCWT can effectually decouple the generator from the grid, thereby improving its fault response. This turbine can also be operated at a wide rotor speed range, thereby extracting power from wind more

efficiently compared with other turbines. However, the converter that connects FWCT to the grid handles the entire output of the generator, thereby explaining the high cost and high-power loss of FCWTs. Nevertheless, these turbines provide a large amount of space for supplying reactive power to the grid. As another advantage, the permanent magnet alternator (PMA) does not have rotor windings, thereby minimizing excitation losses and reducing the size of the generator, which is impossible in the other three types of turbines. The absence of slip rings also helps reduce the maintenance cost of these turbines. Given these features, FCWT PMA wind turbines have been employed in offshore wind power plants.

PMA is usually deployed to the grid by converting AC to DC and vice versa. The AC to DC converter is formed by a diode bridge rectifier, and the buck boost converter controls the DC link voltage. The DC to AC conversion is achieved by a current controlled inverter that controls the active and reactive power.

Given these advantages, an FWCT is integrated into the HVDC transmission link in this thesis.

1.7 HVDC Transmission Control Methods

Converters play a major role in HVDC transmission systems as they are primarily responsible for converting AC into DC or vice versa and for ensuring an efficient control of the power flow.

The conventional LCC-HVDC technique requires the operation of synchronous voltage. The converters are operated by delaying the current waveform ideally between 0 and π rad with respect to the voltage waveform. Therefore, the current always lags the voltage and absorbs reactive power. The commutation process in LCC also

produces considerable harmonic contents. Therefore, these systems demand reactive power from filters and shunt banks, which should be part of the converter stations, thereby increasing their footprints. LCC-HVDC also faces difficulties when connecting to weak grids.

To ensure a stable operation, the classic LCC transmission should be connected to a PC on an AC grid with a short circuit power that is at least 2.5 times the rating of HVDC (Andersen, 2006).

The VSC-HVDC system can be used to avoid these drawbacks and to achieve other benefits, such as an independent control of active and reactive power. The VSC can even operate in a weak grid depending on the employed control algorithm and requires less footprint. Several methods are used to establish this control, including direct method or power angle control, vector current control, power synchronization control, and synchronverter control. These control methods are reviewed in detail below.

1.7.1 Power Angle Control

The power angle and vector current controls are two of the most extensively investigated control methods (Svensson, 1998). Both these methods employ a d-q coordinate system. The power angle control used based on a system model in steady state and can be easily implemented due to its simplicity. The active power is controlled by the phase angle shift between the VSC and AC systems, whereas the reactive power is controlled by changing the magnitude of VSC voltage (Ooi & Wang, 1990). They describe the implementation of voltage amplitude, voltage angle, and frequency controls in a boost-type PWM converter. By using the voltage angle lock loops, converters act as either power dispatchers or voltage regulators in a multi-terminal HVDC system. They presented the experimental results for a 1 kVA size

model and shows that the characteristics of boost-type PWM converters can be adapted to improve the flexibility of HVDC stations. The application of power angle control for HVDC, static synchronous compensators (STATCOM), and wind turbines have been investigated (Joos et al., 1991). One of its drawbacks lies in the control bandwidth, which is limited by the resonant peak at the grid frequency. Another drawback is that the control system is incapable of limiting the current flow to the converter. Among these problems, the latter is particularly serious given that the VSC cannot withstand overcurrent. Therefore, the control should limit the valve current to avoid tripping the converter at disturbances. Power angle control maintains the voltage phase angle of VSC to change the active power, whereas reactive power control changes the voltage magnitude of VSC (Zhang et al., 2010). Power angle control was eventually replaced by vector current control due to its inability to regulate the current flow into the converter and its limited control bandwidth. Given that VSC does not provide any overcurrent capability, the current flowing into the converter can reach very high levels.

1.7.2 Vector Control

The vector current control has become the most dominant control method for grid-connected VSCs due to its successful applications in ASDs, and DFIG wind turbines etc. (Kazmierkowski & Malesani, 1998). The vector current control adapted by Svensson (1998) is a current-control-based technology that limits the current naturally flowing to the converter during disturbances. As its basic function, the vector current control independently controls instantaneous active and reactive power through a fast-inner current control loop. The vector control decomposes the currents into two orthogonal components and controls the power by controlling these components with

a fast-inner current control loop. With the help of the phase locked loop (PLL), the current is decomposed into d and q axis currents, which correspond to active and reactive power controls, respectively. The direct voltage is controlled by an outer loop through the d component, whereas the reactive power control is achieved by the q component. Therefore, the control structure has two loops, namely, an inner current control loop and an outer power control loop that generates the current reference for the inner loops.

Some challenges being faced by VSC-HVDC based on vector current control in weak AC system connections are listed in Konishi et al. (2001) and Durrant et al. (2003). Low frequency resonance is one of the most common problems that can interfere with the fast inner current control loop, thereby limiting the VSC control performance (De Toledo, 2007.; Harnefors, Bongiorno, & Lundberg, 2007). Another problem is that PLL dynamics may have a negative impact on the performance of VSC-HVDC in weak AC systems (Durrant et al., 2003; Jovcic et al., 2003).

The vector-controlled VSC is highly stable under grid disturbances, has inherent protection against overcurrent, can control line harmonics, and can address other quality concerns (Abdel-Galil et al., 2007). However, this VSC faces other problems when connected to weak AC grids. For instance, the performance of converters is limited by the interference of the fast inner current loop and the low-frequency resonance (Harnefors et al., 2007). Nevertheless, vector-controlled VSC has major applications in DFIG wind turbines, adjustable drive inverters, and VSC-connected grids (Kazmierkowski & Malesani, 1998; Svensson, 1998).

The real pattern in the controlling strategy for HVDC-VSC links depends on the entrenched vector control scheme. Hammad and his team (1990) modified the standard

vector control to improve the dynamic performance of parallel AC/DC interconnection. Given that VSCs can be connected for weak AC systems but not for conventional thyristor-based HVDC, a special control technique must be employed. An optimal control strategy was developed by using the direct current vector control mechanism for an HVDC light system (Li et al., 2010). A decoupled PI controller with independent control over active and reactive power can determine the operating characteristics of VSC-HVDC. The incapability of the conventional control mechanism was analyzed through a theoretical study and software simulation. When the controller operates beyond the PWM saturation limit, the conventional technique can lead to overvoltage and system oscillation.

Figure 11 presents the schematic diagram of the VSC-HVDC system using the vector current control.

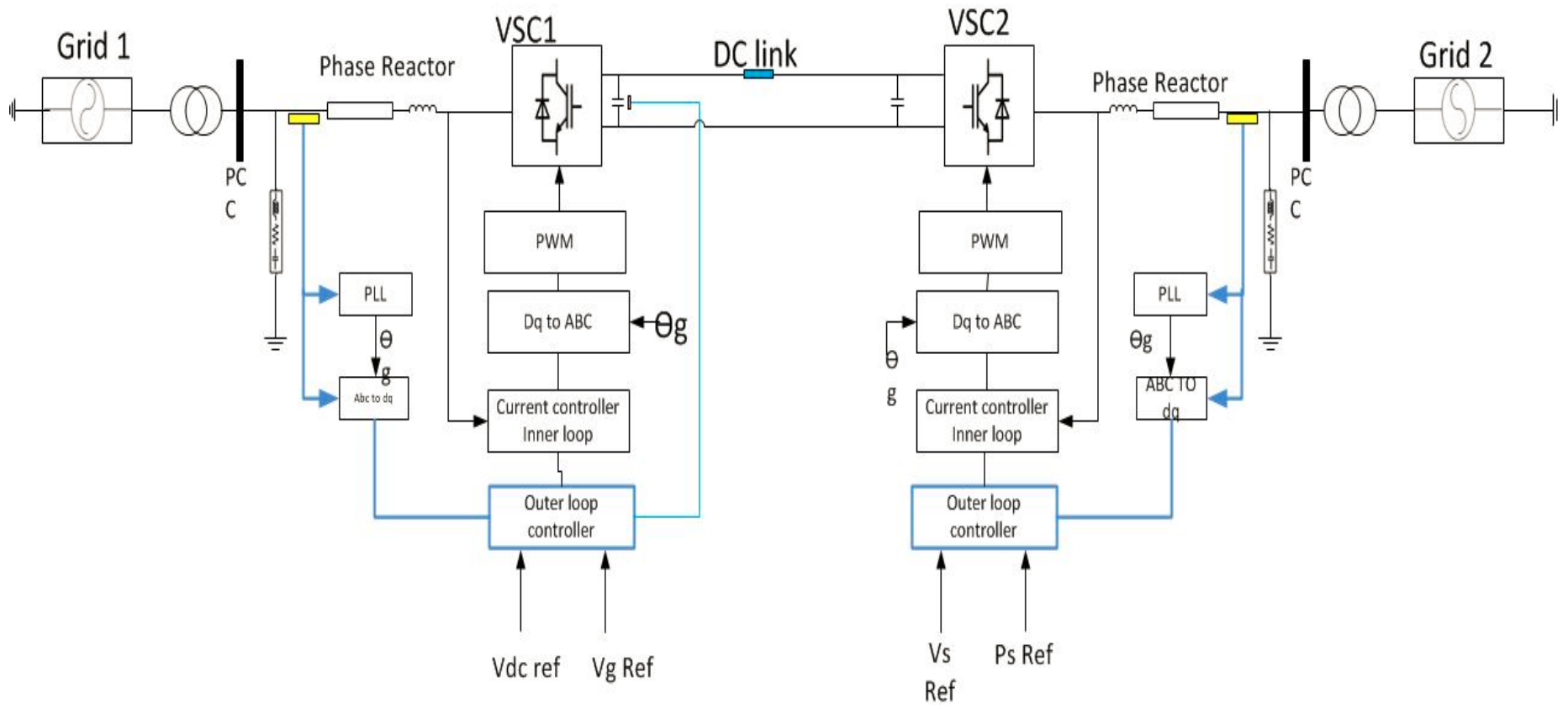


Figure 11: VSC Conventional Vector Control Approach

1.7.2.1 VSC-HVDC Transmission by Vector Control Approach

In HVDC transmission, the active power of the grid is transmitted through the DC link with the help of converters. The reactive power cannot be exchanged through DC links and is only exchangeable on the AC sides. In other words, one side of the HVDC system is meant to control the DC voltage, whereas the other side is used to control the active power. The vector control enables the system to control the active and reactive power independently. Therefore, both sides of the station can control the voltage at PCC, control the reactive power, or regulate the unity power factor. Figure 13 shows the arrangement for controlling the voltage at PCC for both stations. VSC 1 is designed to control the DC voltage, whereas VSC 2 is set for the active power control. The d q frame and PI controller are used to implement this control system.

Figure 12 shows the MATLAB model developed for the conventional vector control for HVDC transmission. The HVDC sending station is set for the active power control, whereas the HVDC receiving station is designed to control the DC voltage.

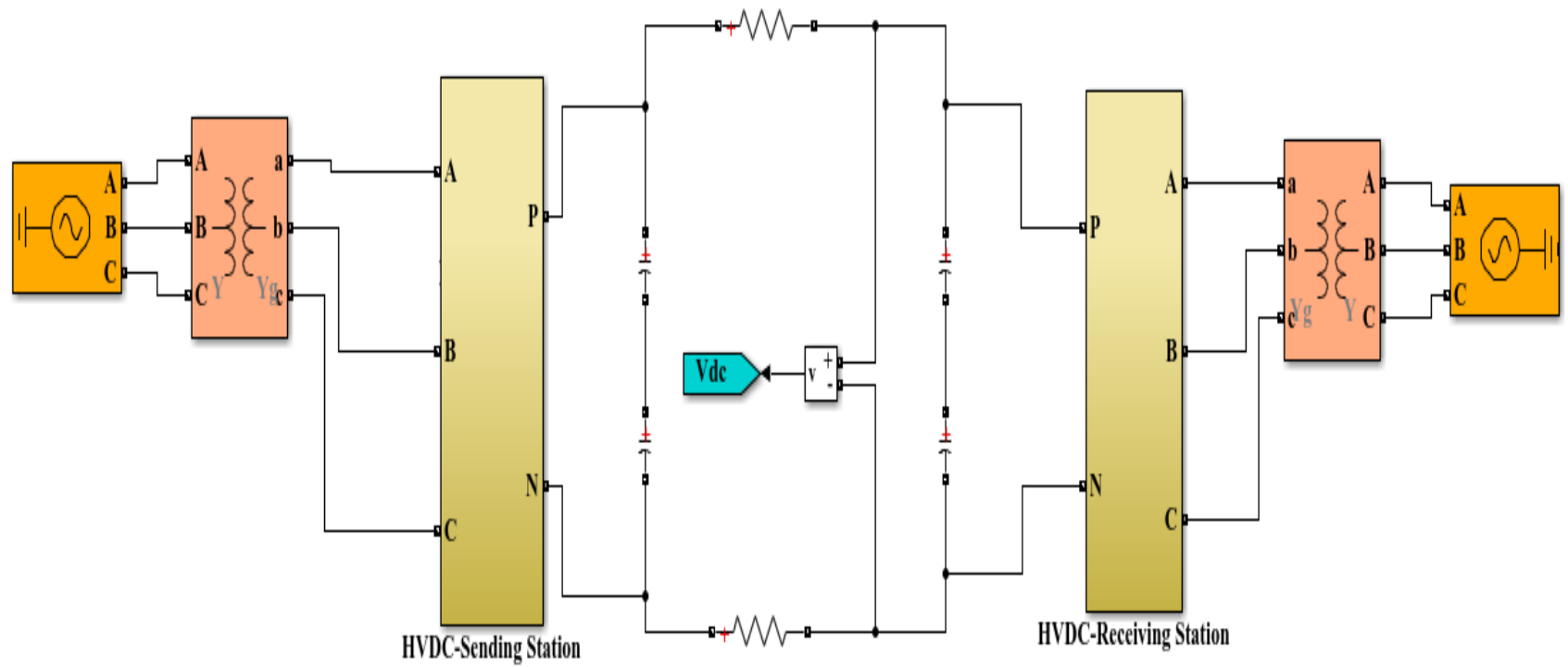


Figure 12: Conventional Vector Control Method for HVDC Transmission.

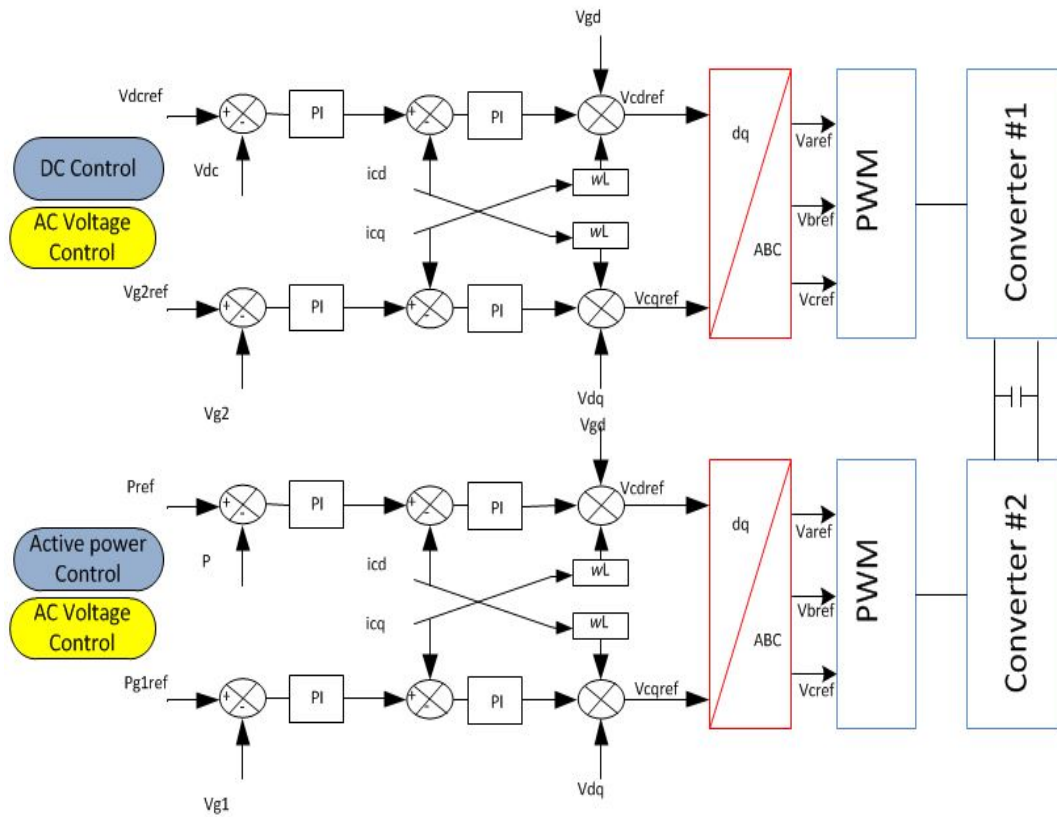


Figure 13: Control and Structure of the VSC-HVDC System

The model shown in Figure 13 illustrates the generation of the reference signal for VSC (Alawasa, 2016). The dynamic equations in the synchronous frame rotating with the grid voltage are

$$V_{cd} = \left(R i_d + L \frac{d i_d}{dt} \right) + (v_{gd} - \omega L i_q) \quad (1.2)$$

$$V_{cq} = \left(R i_q + L \frac{d i_q}{dt} \right) + (V_{gq} + \omega L i_d) \quad (1.3)$$

The error signal obtained by comparing V_{dcref} with V_{dc} is fed to the PI controller to yield the reference signal i_{dref} . This reference signal is then compared with i_d before being fed to the PI controller, and the generated signal is then added to V_d (from the grid voltage by using PLL). The result is then compared with i_q (multiplied by a gain).

A similar approach is used to obtain the q component. The resultant vector is converted from d q to an abc frame, which is then fed as gate pulse to VSC to control the DC link voltage. The same approach is used to generate the switching signal of VSC that controls the active power. The only difference is that i_{dref} is generated by comparing P_{ref} with the actual active power.

The conventional vector control method applied for VSC-HVDC acts similar to a constant voltage source due to the absence of an inertia effect in the system when connected to a weak grid. The stability may be affected during transient conditions (Rajan & Amrutha, 2017). The synchronverter approach is more stable due to the inertia effect of the synchronous mechanism. Therefore, the synchronverter approach is adopted in this thesis for the VSC-HVDC system.

1.7.3 Power Synchronization Control

The drawbacks of vector control when connected to weak AC grids are addressed by power synchronization control. Similar to power angle control, power synchronization control also uses power angle and voltage magnitude to control active and reactive power (Zhang et al., 2010).

Unlike other control methods, the power synchronization control utilizes the internal synchronization mechanism in AC systems and, in principle, follows the operation of a synchronous machine (SM). By using power synchronization control, the VSC avoids the instability caused by the standard phase-locked loop in a weak AC system connection. Moreover, a VSC terminal can provide strong voltage support for the weak AC system similar to a normal SM. Therefore, power synchronization control does not require the short-circuit capacity of the AC system to be connected and allows either

a strong or weak short-circuit capacity. Meanwhile, VSC-HVDC provides strong voltage support to the weak AC system similar to a normal SM.

However, a weak AC system connection still presents a more challenging operating condition for VSC-HVDC compared with a strong AC system connection due to its relatively higher load angles. Therefore, when using power synchronization control, the VSC-HVDC should run with a control system with a lower bandwidth when connected to a very weak AC system to maintain a safe stability margin.

1.7.3.1 Power Synchronism Mechanism

Figure 14 shows the synchronization mechanism of a simple system that comprises two SMs denoted by SM1 and SM2. The power flows from SM1 to SM2 under the assumption that the former operates as a synchronous generator (SG) whereas the latter operates as a synchronous motor. Let X be the sum reactance of both SMs and the line interconnecting these machines. All resistances and other damping effects are disregarded.

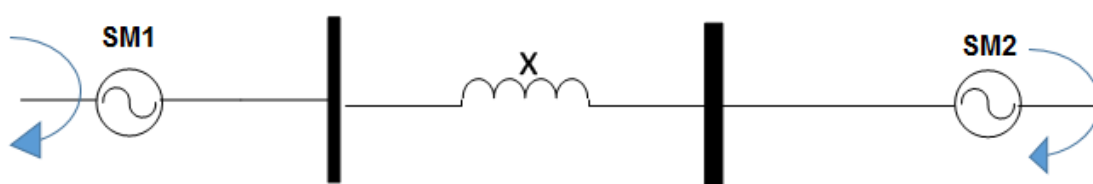


Figure 14: Synchronization Mechanism Between Two Synchronous Machines in AC System

The two SMs initially operate at a steady state as shown in the phasor diagram in Figure 15. E_1 and E_2 denote the phasors that represent the line-to-line equivalents of the inner

EMFs of the two SMs and are always assumed to be constant. The electrical power transmitted from SM1 to SM2 can be computed as:

$$P = \frac{E_1 E_2 \sin \theta}{X} \quad (1.4)$$

where θ is the electrical angle separating the EMFs E_1 and E_2 .

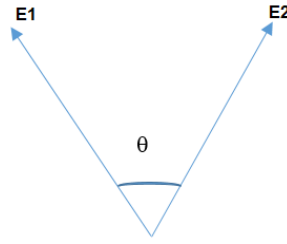


Figure 15: Phasor Diagram Synchronization (Steady State)

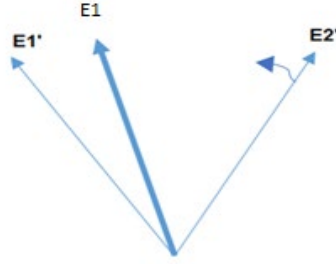


Figure 16: Phasor Diagram Synchronization (Phase Shifting of an Equivalent Inner EMF)

The mechanical torque T_{m_1} of SM1 increases and then returns to its initial value within a short period. In this case, the mechanical angle of the SM rotor moves forward according to the following swing equation (1.5):

$$J_1 \frac{d\omega_1}{dt} = T_{m_1} - T_{e_1} \quad (1.5)$$

where J_1 is the inertia of the shaft system of SM1, ω_1 is the rotor speed, and T_{e_1} is the electromechanical torque of SM1. The change in the mechanical angle of rotor SM1 can change in the emf of SM1 as denoted by E_1' in Figure 16. As a result, the phase

difference between the two SMs increases. In other words, the swing equation increases the power transmitted from SM1 to SM2. The increase in electrical power is equal to the increase in electromechanical torque T_{e_2} of SM2. Assuming that SM2 provides a constant load torque T_{m_2} , the SM2 rotor accelerates according to the following equation:

$$J_2 \frac{dw_2}{dt} = T_{e_2} - T_{m_2} \quad (1.6)$$

Where, J_2 is the total inertia of the shaft system of SM2, and w_2 represents the mechanical angular velocity of SM2. As the rotor of SM2 accelerates, the phase of E2 moves as shown in Figure 16. Therefore, the phase difference in the EMFs of these two SMs decreases. When a transient occurs in a real situation, a considerable amount of damping is observed. The system returns to its steady state when the phase difference in the EMFs of the two SMs returns to its initial value.

In sum, the SMs can operate in various AC networks where the vector current control method fails.

1.8 DC Link Capacitor

The change in the polarity of the DC bus has no scope given that the DC link capacitor acts as a voltage source in HVDC transmission. The DC link capacitor plays a major role in maintaining the DC voltage to its required level. Choosing the appropriate value of the DC link capacitor is a challenging task that involves determining the transient response of the system. As the current with harmonics generated from PWM switching of IGBTs, flowing to capacitor creates a voltage ripple at DC side. The size of the capacitor cannot be determined in a steady state operation as it leads to a DC

overvoltage. The transient overvoltage constraint should be considered when choosing the DC capacitor value (Du, 2007).

The Time constant τ determines the time required to charge the DC capacitor from zero to its DC voltage level at the nominal apparent power of the converter (Du, 2007; Jian Luo et al., 2011).

$$\tau = \frac{1}{2} \frac{C U_{dc}^2}{S_n} \quad (1.7)$$

where U_{dc} is the DC link voltage and S_n is the nominal apparent power.

1.9 Synchronverter

Zhong & Weiss (2011) proposed a control method that operates an inverter by mimicking the behavior of an SG. The resulting control loop is called a synchronverter. The operational concept of AC systems by SGs voltage and frequency is well established. Consequently, the synchronverter concept has many applications that have been well documented in the literature. For instance, Phi-Long Nguyen and his team (2012) developed a synchronverter-based operation of STATCOM, Zhou Wei et al. (2015) performed a small signal modelling and analysis of a synchronverter by using a laboratory prototype set up of 5kW + 5kVAR, and Ferreira et al. (2016) proposed a single phase synchronverter for residential generators.

Meanwhile, Aouini, et al. (2016) introduced an HVDC transmission control strategy based on the synchronverter concept. Specifically, they proposed a specific method for tuning the parameters of SMs to improve the adaptability of controlling HVDC transmission. Rajan and Amrutha (2017) compared the synchronverter-based HVDC transmission with the conventional vector control method. Given that the disadvantages of VSC-HVDC transmission can be addressed by a synchronverter, a

synchronverter based HVDC transmission can be used for transmission without worrying about the nature of the grid. Therefore, synchronverter based HVDC can play a leading role in the integration of remote RES into existing AC grids.

1.10 Renewable Energy Integration

RES, such as solar and wind energy, have been used to meet the increasing energy demand in a sustainable manner. These energy sources are environmentally friendly and are crucial in generating electricity. However, they are located too far from the main AC grid, and their power output depends on the climate. Among multiple types of RES, wind energy is the fastest-spreading renewable energy technology. Therefore, technologies for harvesting wind energy and generating electricity have been extensively investigated in the literature. The challenges faced in transmitting wind power over long distances are discussed in detail in this study.

Some problems are encountered when transmitting power from wind farms over a long distance. Generally, the machine connected to a wind turbine can be a PMSG, induction generator, or DFIG. A DFIG requires two special converters to be integrated into the AC system, whereas the output of PMSG, which is AC in nature, can easily be converted into DC. Therefore, depending on the type of windfarm, another set of AC to DC converters may be needed for the integration. The variances in wind power may also lead to oscillations in the power system, which can pose a serious problem.

The main drawback of wind energy lies in its varying output power, which can be ascribed to the variations in wind speed and result in poor power quality.

Many studies have examined how the power generated from wind energy can be stabilized. For instance, Torres et al., 2012 investigated the feasibility of using a hybrid

HVDC transmission system for integrating offshore wind farms. This technology is based on two types of converters, namely, PWM CSC and LCC, which are placed offshore and onshore, respectively. For grid-connected and DFIG-based wind energy conversion systems, Ganti and his team (2012) proposed a new control strategy that employs a battery energy storage system (BESS) to mitigate the power fluctuations on the grid resulting from the unpredictable nature of wind.

Many studies on HVDC transmission lines and the synchronverter concept have been conducted. Some of these studies have been published in the field of wind farm generation and introduced certain control strategies. Their findings all show that power fluctuations can be improved by introducing battery banks to a wind system.

This thesis uses the synchronverter concept to establish a stable HVDC power transmission system between two grids wherein the DC link is integrated into an RES (wind farm) given the large amount of RES in such areas.

1.11 Problem Statement

As the demand for energy increases each day, people have turned to RES to meet such demand. These sources are more reliable and cost effective than traditional energy sources and provide an ecofriendly atmosphere that helps prevent adverse environmental conditions. While electrical power systems used to depend on centralized generating stations, the advancements in technology have allowed the integration of an increasing number of distributed energy generating stations into power system networks. Most of these stations use RES, including solar and wind energy, and comprise variable frequency AC or DC sources, thereby requiring the integration of many converters into the system. However, doing so can lead to the

instability of electrical grids. To solve these problems, an efficient generation and transmission of electrical power must be guaranteed.

Given the dominance of distributed energy sources in a power network, a model that integrates various distributed energy sources (generally RES) into a HVDC transmission system must be developed.

In this thesis, the VSC-HVDC transmission between two AC grids that are integrated into a wind farm is analyzed, and an auto regulation of power control among the three based on the set factor demanded by any of the two grids. A synchronverter is utilized to control the power in this network given that the SG voltage/frequency is a well-established operational concept in AC grids.

1.12 Objective

The main objectives of the thesis are to:

- a) Develop and test a synchronverter-based HVDC transmission system,
- b) Integrate an RES directly into the DC link of HVDC transmission, and
- c) Integrate BESS into the DC link to mitigate the power oscillations resulting from the variations in wind power.

1.13 Scope of Work

The study examines the application of the synchronverter concept in HVDC transmission and develops an efficient control strategy for transferring power between two grids. To achieve these ends, a control loop that mimics the converters to that of an SM is developed, and an VSC-HVDC transmission is implemented.

The voltage source converter is controlled by generating a back EMF by using an SM. The average model-based VSC is fed with a PWM signal to the VSC for switching of valves which develop a corresponding DC signal and is transmitted to another end converting station where the DC signal is converted back to AC to feed to the AC grid. A wind farm is integrated into the HVDC transmission link by initially modelling a type 4 wind farm and by integrating this source into the HVDC transmission link between two AC grids.

The power flow between two grids and the wind farm is then analyzed. The power generated by the wind farm is monitored, and a reference power is set for the receiving end. The power received at the receiving station is compared with the total power at the sending station and with the power generated at the wind farm.

1.14 Summary

This chapter presents the various aspects of the HVDC transmission system, specifically VSC-HVDC transmission.

The first part highlights the importance and background of HVDC transmission. The second part introduces the basic components of an HVDC system and lists the advantages of HVDC transmission over HVAC transmission. Different HVDC system configurations are also described.

The conventional HVDC transmission is then compared with VSC-HVDC transmission, and the advantages of the latter over those of CSC-based transmission are enumerated. The VSC-HVDC link structure is illustrated, followed by an explanation of various wind turbine configurations and types.

The synchronverter concept and the methods for controlling HVDC transmission are then discussed in detail. The feasibility of integrating RES into the VSC-HVDC transmission system is explained, and the importance of this study is elaborated. The chapter ends by presenting the objectives and research scope of this thesis.

Chapter 2: Modelling and Control Techniques

2.1 Modeling of Synchronous Machines

The modeling concept of SMs is adapted from Zhong and Weiss (2011) as well as Younis and his team (2018). An SM is considered a passive dynamic system without any specific assumptions on the signals. All stator inductances are kept constant by using a round rotor machine. The model has one pair of poles per phase and one pair of poles on the rotor under the assumption that no damper windings, magnetic saturation effects in the iron core, and eddy currents are present.

The field and three identical stator windings are distributed in slots and the periphery of a uniform air gap. The stator winding has a self-inductance L and mutual inductance $-M$ with a value $-0.5 L$ as shown in Figure 17 (Zhong & Weiss, 2011). The field winding has a self-inductance L_f and the mutual inductance formed between stator and field coils changes along with rotor angle θ and is represented by equations (2.01) to (2.03). Figure 17 illustrates the structure of an idealized three phase round rotor SG.

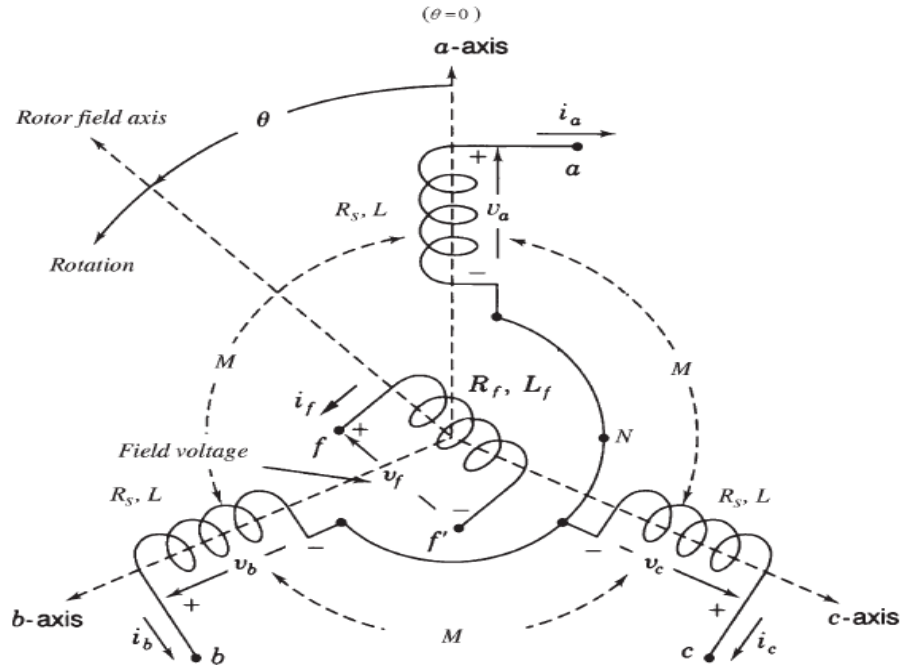


Figure 17: Structure of idealized three phase round rotor SG.

$$M_{a,f} = M_f \cos(\theta) \quad (2.01)$$

$$M_{b,f} = M_f \cos(\theta - 2\frac{\pi}{3}) \quad (2.02)$$

$$M_{c,f} = M_f \cos(\theta - 4\frac{\pi}{3}) \quad (2.03)$$

where $M_f > 0$

The flux linkage of the windings is formulated as

$$\Phi_a = Li_a - Mi_b - Mi_c + M_{a,f}i_f \quad (2.04)$$

$$\Phi_b = Li_b - Mi_a - Mi_c + M_{b,f}i_f \quad (2.05)$$

$$\Phi_c = Li_c - Mi_b - Mi_a + M_{c,f}i_f \quad (2.06)$$

$$\Phi_f = L_f i_f + M_{b,f}i_b + M_{a,f}i_a + M_{c,f}i_c \quad (2.07)$$

where i_a, i_b, i_c are currents in the stator and i_f is the rotor excitation current,

To simplify the equation,

$$\Phi = \begin{bmatrix} \Phi_a \\ \Phi_b \\ \Phi_c \end{bmatrix} \quad (2.08)$$

$$i = \begin{bmatrix} i_a \\ i_b \\ i_c \end{bmatrix} \quad (2.09)$$

$$\widetilde{\cos(\theta)} = \begin{bmatrix} \cos(\theta) \\ \cos(\theta - 2\frac{\pi}{3}) \\ \cos(\theta - 4\frac{\pi}{3}) \end{bmatrix} \quad (2.10)$$

$$\widetilde{\sin(\theta)} = \begin{bmatrix} \sin(\theta) \\ \sin(\theta - 2\frac{\pi}{3}) \\ \sin(\theta - 4\frac{\pi}{3}) \end{bmatrix} \quad (2.11)$$

Assuming the neutral is not connected then,

$$i_a + i_b + i_c = 0 \quad (2.12)$$

The flux linkage of the stator is formulated as

$$\Phi = L_s i + M_f i_f \widetilde{\cos(\theta)} \quad (2.13)$$

Where,

$$L_s = L + M \quad (2.14)$$

The flux linkage of the field is formulated as,

$$\Phi_f = L_f i_f + M_f \langle i, \widetilde{\cos(\theta)} \rangle \quad (2.15)$$

where $\langle \cdot, \cdot \rangle$ denotes the conventional inner product in \mathbb{R}^3 , $M_f \langle i, \cos(\overline{\theta}) \rangle$ is the armature reaction that remains constant when the three phase currents are sinusoidal and balanced, and $\sqrt{\frac{2}{3}} \langle i, \cos(\overline{\theta}) \rangle$ is the d- axis component of the current.

The resistance of the stator winding is denoted by R_s , and the phase terminal voltage v is computed as

$$v = -R_s i - \frac{d\Phi}{dt} = -R_s i - L \frac{di}{dt} + e \quad (2.16)$$

Where $v = \begin{bmatrix} v_a \\ v_b \\ v_c \end{bmatrix}$ and $e = \begin{bmatrix} e_a \\ e_b \\ e_c \end{bmatrix}$ and e is the electromotive force resulting from rotor movement. This force is also known as no load voltage or synchronous voltage.

$$e = M_f i_f \dot{\theta} \sin(\overline{\theta}) - M_f \frac{di_f}{dt} \cos(\overline{\theta}) \quad (2.17)$$

The field terminal voltage can be computed as

$$v_f = -R_f i_f - \frac{d\Phi_f}{dt} \quad (2.18)$$

where R_f is the resistance of the rotor winding.

However, i_f is used instead of v_f in this thesis as a constant adjustable input.

The mechanical part of the machine is governed by,

$$J\ddot{\theta} = T_m - T_e - D_p \dot{\theta} \quad (2.19)$$

where J is the moment of inertia of all the parts rotating with the rotor, T_m is the mechanical torque, T_e is the electromechanical torque, and D_p is the damping factor.

When constant flux linkages are considered, no back EMF is produced. Therefore, all power flow is mechanical. The torque T_e can be derived from energy stored in electromagnetic field “E” as

$$T_e = -\frac{\partial E}{\partial \theta} \quad (2.20)$$

When i, i_f are constant (constant flux linkages),

$$T_e = -M_f i_f \left\langle i, \frac{\partial \cos(\theta)}{\partial \theta} \right\rangle = M_f i_f \left\langle i, \sin(\theta) \right\rangle \quad (2.21)$$

If i_f is constant, then according to equations (2.17) and (2.21),

$$T_e \dot{\theta} = \langle i, e \rangle \quad (2.22)$$

2.2 VSC-HVDC Transmission System Configurations

Figure 18 presents the schematic diagram of the main circuit of the voltage source converter. The switches are of IGBT type. A symmetrical three phase load with impedance $R + j\omega L$ is connected to EMFs $e_1(t), e_2(t)$ and $e_3(t)$. The star connected neutral point has the potential of $V_0(t)$ due to a floating ground. $V_1(t), V_2(t)$ & $V_3(t)$ are the phase potentials of VSC. The current flowing from DC link to the converter is denoted as $I_v(t)$, the current flowing through DC link is denoted by $I_{dc}(t)$ and the DC link voltage across the DC link capacitor is denoted as $U_{dc}(t)$.

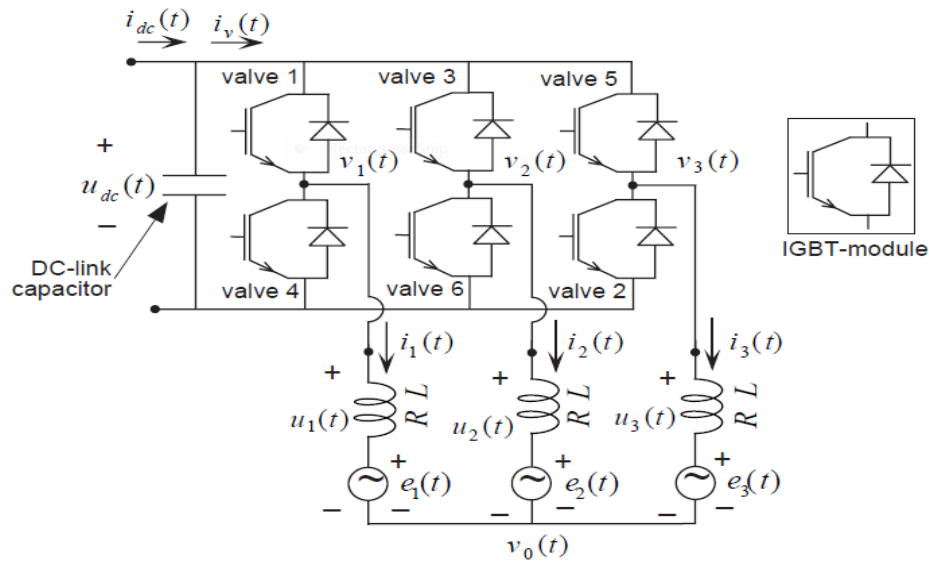


Figure 18: VSC Structure

2.3 Synchronverter-Based HVDC Control

The increased generation of distributed energy sources such as wind, solar, and other RES, has resulted in the integration of converters (e.g., AC to DC or DC to AC) to the public grid. For example, the wind turbines which generate free energy at variable frequencies requires conversion from AC to DC and back to AC to supply the grid. Meanwhile, the photovoltaic arrays require a DC to AC conversion. The overall stability of the grid is affected when using a large number of distributed generating stations that supply a considerable amount of power to the grid. A large number of distributed generating stations also requires an effective control of power flow such as in the case of conventional power generators. Since we have, a well-established theory developed for SGs driven by prime movers it is easier, if we can develop a control strategy like the one we use already for conventional generators or redesign the power system network to operate in a different way by implementing fast communication lines between the machines and centralized control stations. In this thesis, we choose the existing control system and the synchronverter concept.

2.3.1 Synchronverter

The idea of mimicking the operation of an inverter to that of a SG has resulted in the development of the synchronverter concept (Zhong & Weiss, 2011). Through this concept, the well accepted algorithms used for controlling SMs can also be utilized to control the power systems with a large number of inverter-based sources. Zhong & Weiss (2011) proposed a method in which the inverter operates by mimicking the behavior of the SG. The dynamic equations are kept the same, whereas the mechanical power exchanged with the prime mover changes to the exchanged power in DC bus. In other words, a synchronverter is an inverter that exchanges power with multiple components of a system, including filter inductors, capacitors, and the related controllers. A synchronverter reflects the positive and negative aspects of an SG. As its major benefit, a synchronverter allows the selection of system parameters, including inertia, friction coefficient, field inductance, and mutual inductance. No real energy loss is recorded in a synchronverter due to the virtual mechanical friction that is redirected to the DC bus. Both the magnetic saturation and eddy current can also be kept at zero magnitude. In sum, those values that are impossible to reach in real SGs can be achieved in a synchronverter, and the parameter values can be changed during the operation of the system.

The idea utilized by Aouini et al. (2016), is adapted to this thesis for the power flow control on a HVDC transmission line by the Synchronverter concept. The concept of the synchronverter is implemented for the control of power on a DC transmission system.

At the sending end, the rectifier controls emulate a synchronous motor, whereas at the receiving end, the inverter emulates an SG. The two converters connected to a DC line

provide a synchronverter HVDC (SHVDC). The droop and voltage regulations in the SHVDC structure are used to define the behavior of the entire SHVDC. Moreover, unlike conventional vector-controlled HVDC, SHVDC can provide inertial support and operate in weak grid conditions.

Figure 19 presents a block diagram of synchronverter-based HVDC transmission.

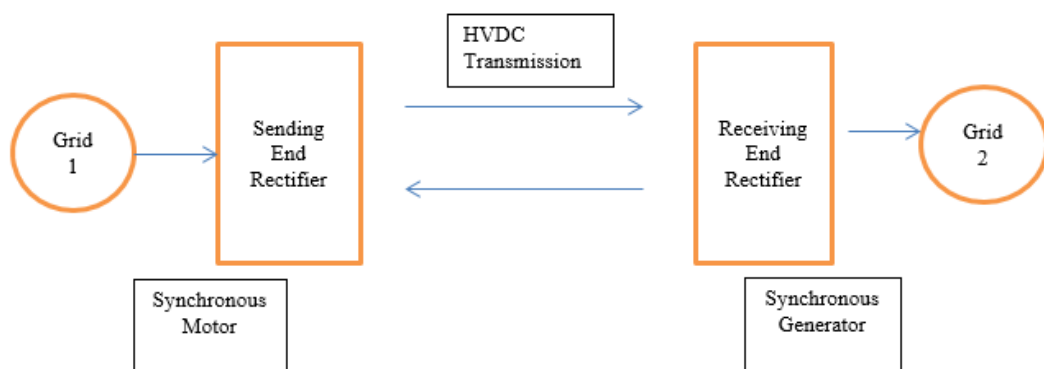


Figure 19: Synchronverter Based HVDC Transmission

2.3.2 Synchronverter Implementation

For easy implementation, a synchronverter can be divided into the power part and the electronic part. The power part includes a three-phase inverter that is operated by using PWM and LC filters that minimize the voltage ripples generated by switching. The grid 1 impedance includes the inductance L_{g1} in series with resistance R_{g1} connected to an infinite bus.

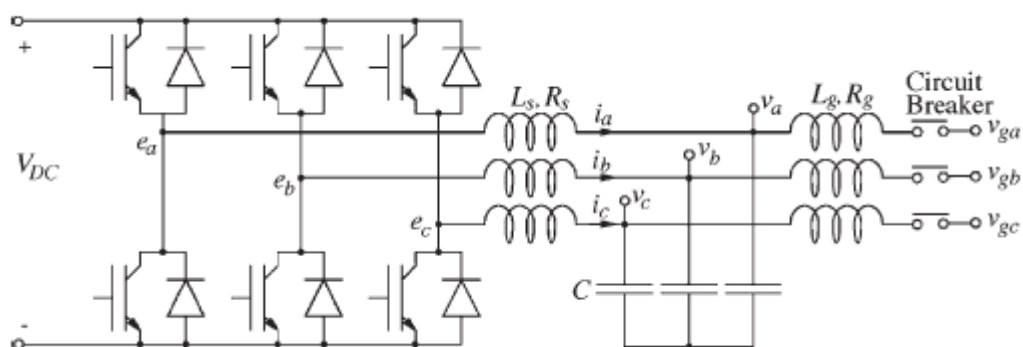


Figure 20: Power part of Synchronverter

Figure 20 shows the power part of a synchronverter. (Zhong & Weiss, 2011), other than 3 sources connected and DC link capacitor connected to another end of the converter. That is the converter along with the impedance RL comprises the power part. This part of the circuit resembles the SG while ignoring the ripples.

Meanwhile, the electronic part of a synchronverter includes a digital signal processor and its associated circuits. This processor switches those valves associated with the converter and runs under a special program that is developed on the basis of the diagram presented in Figure 21. The electronic and power parts of the synchronverter interact via signals e and i . The program in the DSP should also include the control part of the synchronverter.

The voltage of an imaginary SM represents the phase terminal voltage, whereas the impedance of the stator windings of the imaginary SG is represented by inductance L_s and resistance R_s and is assumed to represent the back EMF of a virtual SM. The values of these high-frequency switching signals are averaged. The average value of the back EMFs e_a , e_b , and e_c over a switching period must be equivalent to the value obtained from equation (2.17) by using the PWM technique. If i_f is constant, then equation (2.17) is modified as

$$e = M_f i_f \dot{\theta} \widetilde{\sin(\theta)} \quad (2.23)$$

The values of the capacitors for filtering are chosen such that the resonant frequency is approximately equal to $\sqrt{\omega_n \cdot \omega_s}$, where ω_n is the angular frequency of the grid, and ω_s is the angular switching frequency used to control the switches.

The generated real power and reactive power as viewed from the inverter terminals are computed as

$$P = \langle i, e \rangle \quad (2.24)$$

$$Q = \langle i, e_q \rangle \quad (2.25)$$

where e_q and e are equal in magnitude, whereas the e_q has a phase delay from e by $\frac{\pi}{2}$.

Therefore, from Equation (2.17), we have

$$e_q = M_f i_f \dot{\theta} \widetilde{\sin(\theta - \frac{\pi}{2})} = -M_f i_f \dot{\theta} \widetilde{\cos(\theta)} \quad (2.26)$$

The real power can be expressed as

$$P = M_f i_f \dot{\theta} \langle i, \widetilde{\sin(\theta)} \rangle \quad (2.27)$$

whereas the reactive power of virtual SG is given by

$$Q = -M_f i_f \dot{\theta} \langle i, \widetilde{\cos(\theta)} \rangle \quad (2.28)$$

Equation (2.19) can be rewritten as

$$\ddot{\theta} = \frac{1}{J} (T_m - T_e - D_p \dot{\theta}) \quad (2.29)$$

where the mechanical torque T_m is taken as a control input, and the electrical torque T_e varies according to the values of i and θ obtained from equation (2.21).

The electronic part of the synchronverter is developed based on the basis of equations (2.21) to (2.29) and is shown in Figure 21

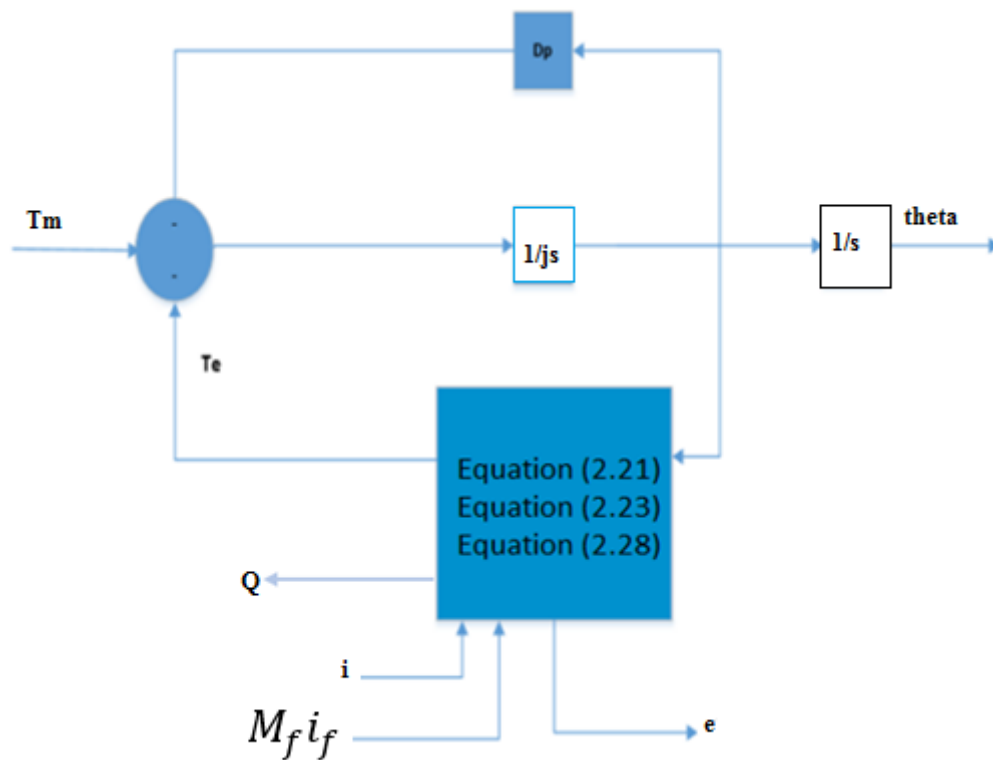


Figure 21: Electronic Part of a Synchronverter

2.4 Battery Energy Storage System Control

The BESS rating is chosen according to the energy storage capability required for the system. The energy required to store only when the power generated by the wind system is greater than the average value of power that is fed to the HVDC link. The average value can be calculated by using the wind speed available to that site. The wind speed varies from one site to another and must therefore be recorded in experiments. The average calculated power is taken as the reference power and is fed to the grid. The BESS rating can be computed as

$$E_b = \sum_{j=1}^m P_{nj} t_j \quad (2.30)$$

where P_{nj} is the surplus power at any instant than the average value of Wind power fed to the HVDC link and t_j is the period in which the surplus power is generated.

P_{nj} can be calculated at any time instant as

$$P_{nj} = (P_i - P_a) \quad (2.31)$$

where P_i is the instantaneous power of the wind turbine, and P_a is the average true power fed to the HVDC link.

2.5 Phase Locked Loop

A PLL is a control system in which the phase of an output generated signal relates with that of an input signal. This loop has several types, the simplest of which includes an electronic circuit of a variable frequency oscillator and a phase detector in a feedback loop. The oscillator generates a periodic signal, and the phase of the generated signal is compared with that of the input periodic signal by using a phase detector while adjusting the oscillator to keep these phases matched.

PLL is a phase tracking algorithm whose output is synchronized with its reference input in both frequency and phase (Timbus, 2007). PLL synchronizes the inverter output current with the grid voltage to obtain a unitary power factor. Figure 22 presents a simple PLL model.

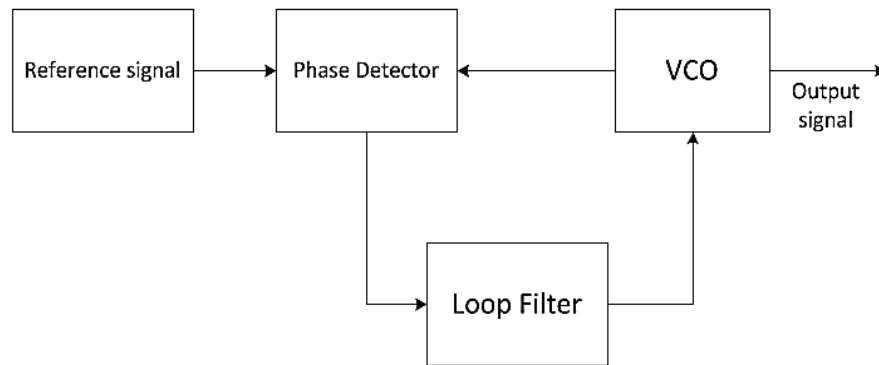


Figure 22: PLL Block Diagram

A block PLL in Simulink is used to extract frequency from the three-phase voltage signal of the grid.

2.6 Boost Converter

A bidirectional boost converter is used to integrate BESS into the DC link of the HVDC. The current flowing through the converter can be controlled to achieve a bidirectional power flow. Figure 23 illustrates a typical bidirectional boost converter, where the output capacitor C_d is the same as the DC link capacitor of the HVDC link.

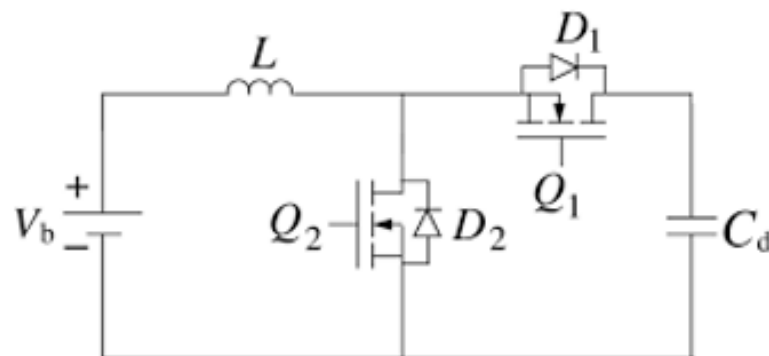


Figure 23: Boost Converter

2.7 Summary

This chapter discusses the modelling and controlling techniques employed in this thesis. The modelling of the SM is initially described in detail. A synchronverter-based control of HVDC is then discussed along with the importance of the synchronverter concept. The synchronverter implementation, BESS control, PLL, and boost converter are also discussed.

Chapter 3: Extension of the Synchronverter Concept for the Auto Regulation of Power Flow Between Two Grids.

This chapter presents in detail the control of power flow between two asynchronous grids, the modeling of a type 4 wind farm, the integration of this wind farm between two grids, and the auto regulation of power between two grids based on the input energy from wind farms.

The MATLAB model in Figure 24 shows the SM emulation of a VSC-HVDC transmission system. Two asynchronous grids are connected through a HVDC transmission line to exchange power based on the grid demand.

The VSC for the conversion of either AC to DC or DC to AC is operated by a signal from the virtual SM control block. The valves of VSCs are operated by a generated PWM signal from the conceptual SM block. The average model-based voltage source converters with three bridge arms are used. The system parameters and its values are shown in Table 1 below.

Table 1: System parameters and its values.

Parameters	Values
Grid Resistance	0.135ohms p.u
Grid Inductance	0.0005 p.u
Nominal frequency	50 Hz
Rated Power	$200 \cdot 10^6$ VA
Nominal voltage	$50 \cdot 10^3$ V _{rms phase-phase}
DC link voltage	1 p.u

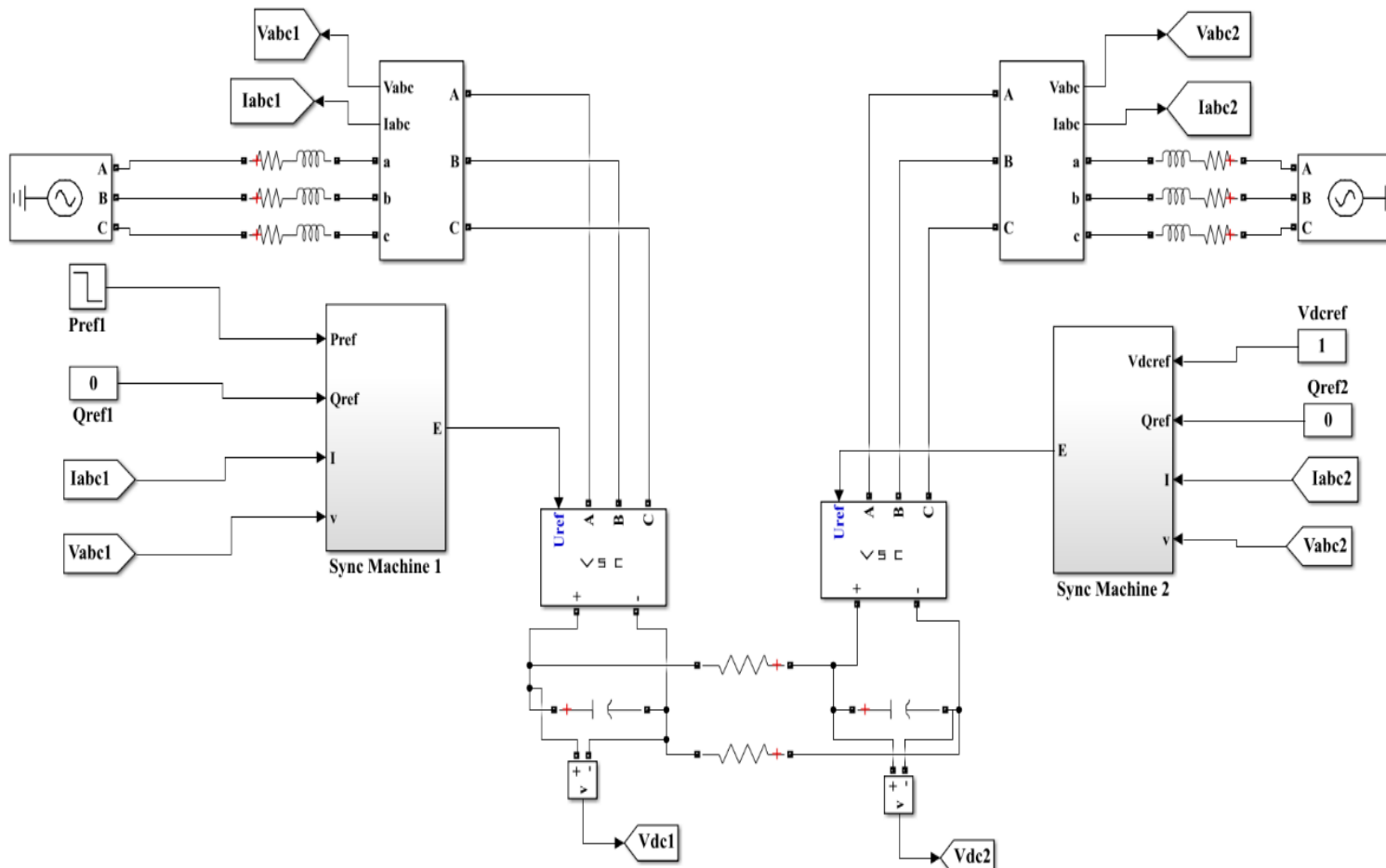


Figure 24: Synchronous Machine Emulation of VSC-HVDC Transmission System

3.1 Power Flow Control between Two Grids by Using a Synchronverter

The left end of Figure 24 is assumed to be the sending end station, whereas that on the right is assumed to be the receiving end station. Therefore, the constant power mode control is adapted to the left end station, and the receiving station is set for the constant voltage mode control. To further understand the power flow, we study the power control in a real SG.

In real SGs, the rotor of the SG is coupled to the prime mover. Therefore, the rotor speed is related to the prime mover. The rotor speed is reduced due to the real power demand and the increase in torque given in equation (2.19). The balance of power is achieved by increasing the mechanical power through a power regulation system associated with the prime mover. The frequency droop control mechanism controls the real power flow between the grid and SGs in the case of sharing loads between SGs.

The aforementioned mechanism can be related to a virtual concept where the virtual angular speed “ $\dot{\theta}$ ” is compared with the angular frequency reference “ $\dot{\theta}_r$,” and the difference is multiplied by a gain to obtain the torque T_m . The impact of the frequency control loop is equal to the increase in the mechanical friction coefficient. As shown in Figure 25, constant D_p includes the total effect of the mechanical friction and frequency droop coefficients. Therefore, we have the change in torque acting on virtual rotor and change in angular frequency by δ shown in equation (3.1).

$$D_p = -\frac{\delta T}{\delta \dot{\theta}} \quad (3.1)$$

The reactive power drawn out of the synchronverter is regulated as

$$D_q = -\frac{\delta Q}{\delta v} \quad (3.2)$$

where D_q is the voltage drooping coefficient, and δQ is the required change in reactive power.

The lower part of Figure 25 presents the control of reactive power. The difference between the reference voltage and V_{amp} is multiplied by D_q and added to the change in reactive power, which is obtained by subtracting reactive power (calculated from current i , θ , and $\dot{\theta}$) from the set reactive power.

Figure 25 presents the active power feedback loop. The reference power can be inputted into the sending end station based on the power demand from the receiving end station while ignoring the losses in the transmission line. The nested structure in the upper part of Figure 25 covers the power part, and the inner loop represents the frequency droop loop. A low pass filter is used to attenuate the ripples produced in the amplitude V_{amp} in the lower part of Figure 25. V_{amp} is calculated as

$$V_{amp} = \frac{-4}{3} \sqrt{(v_a v_b + v_b v_c + v_c v_a)} \quad (3.3)$$

The receiving end control block is similar to the sending end control block except that the former is designed for a constant voltage mode. Figure 26 shows the control loop.

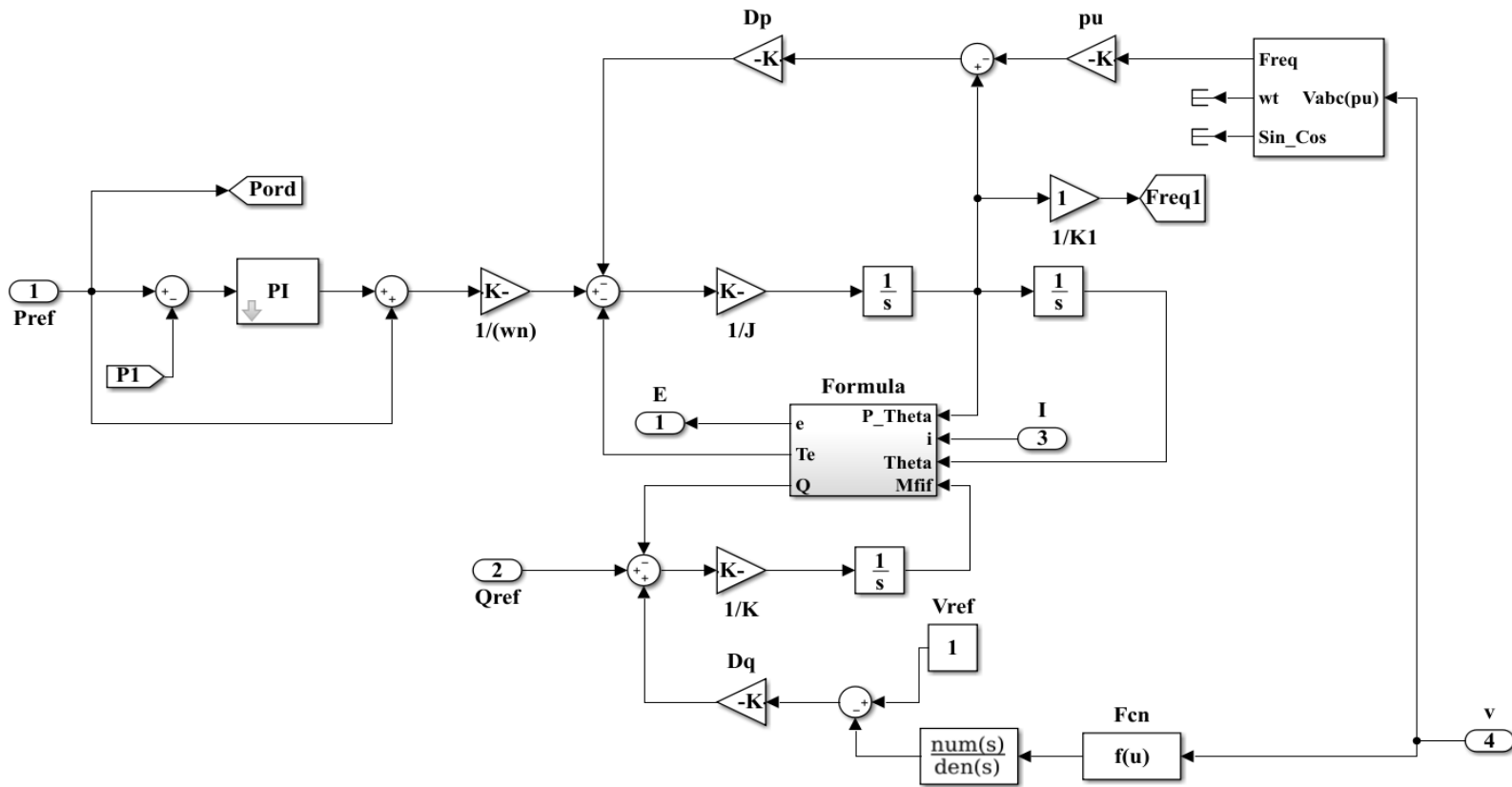


Figure 25: MATLAB Model of the Synchronverter Control for the Constant Power Mode End

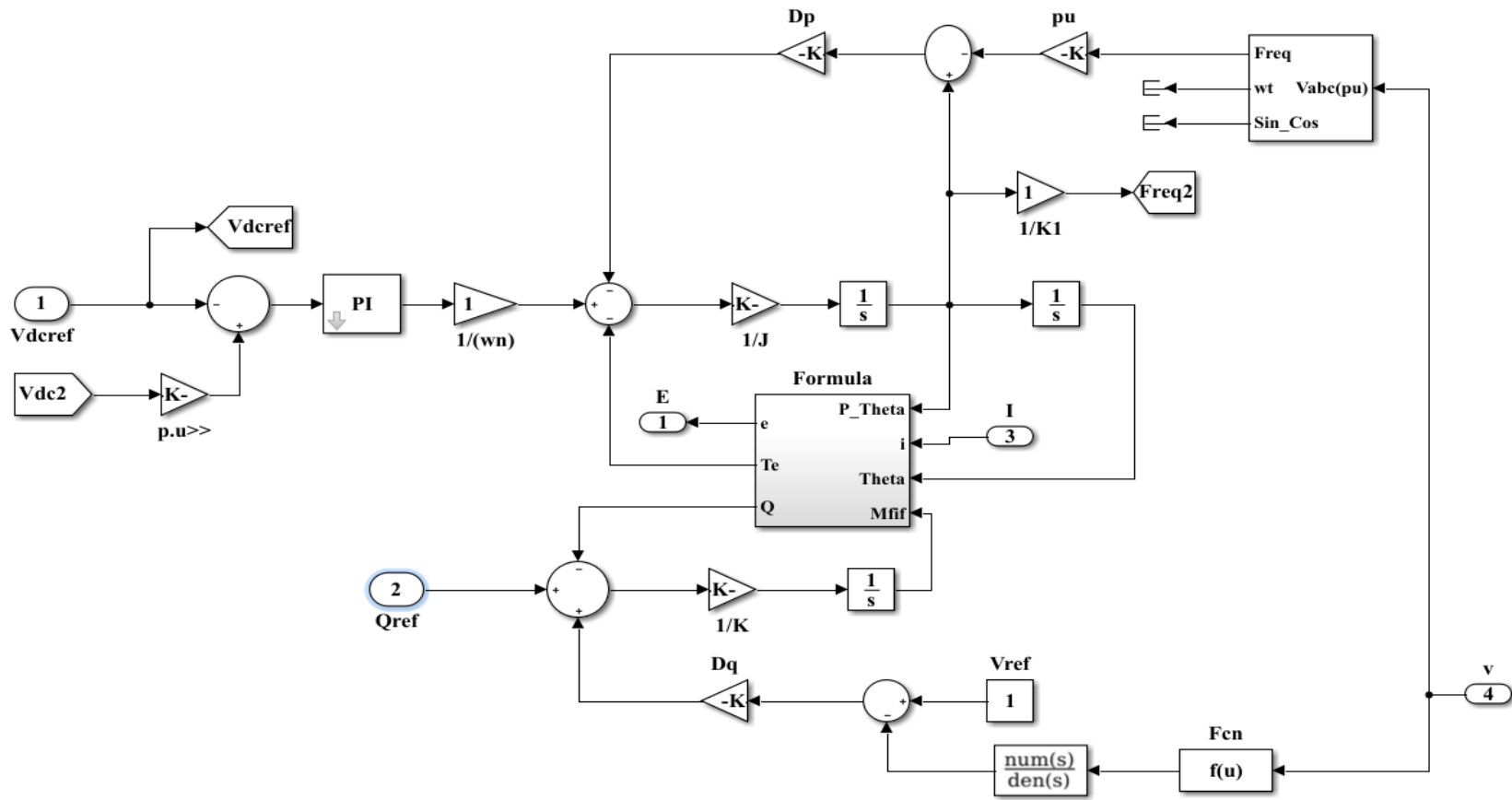


Figure 26: MATLAB Model of the Synchronverter Control for the Constant Voltage Mode End

A PI controller is used in the model for both voltage and power reference control and a Phase locked loop is used to determine the frequency of the grid voltage signal.

3.2 Integration of Type 4 Wind Farm into the HVDC Link

A type 4 wind farm is adopted in this thesis. This type of wind farm uses a permanent magnet SG, where permanent magnets are fixed on the rotor side, and windings are placed on the stator. AC voltage is produced when the machine rotor starts to rotate, and this voltage is converted into DC by using three-phase diode bridge rectifiers. Therefore, depending on the wind speed, the power will be pushed to the DC side. Given that we can directly obtain the DC output, this can be connected directly to the DC link of the proposed HVDC link. Figure 27 presents the MATLAB model of the type 4 wind farm.

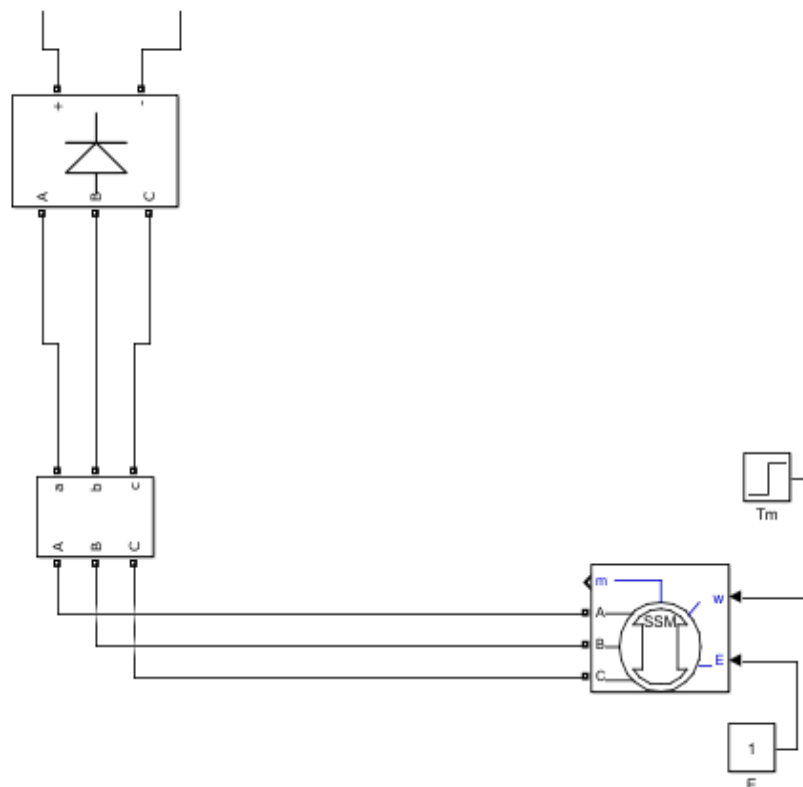


Figure 27: MATLAB Model of a Type 4 Wind Farm

3.3 Integration of Wind Farm Between Two Grids and the Auto Regulation of Power Flow Between Two Grids

The output DC terminals of the wind farm are fed to the HVDC transmission link. The power generated by the wind farm is monitored, and the corresponding power flow from both grids are analyzed in the simulation. Figure 28 presents the final model obtained by integrating the wind farm into the synchronverter-emulated VSC- HVDC transmission system.

To regulate power flow in the absence of a wind turbine in our model, both end stations are equipped with constant voltage and constant real power controls that can be switched according to their power flows. For example, when station 2 (right) demands the power of a certain MW, station 1 (left) operates in constant voltage mode, whereas station 2 operates in constant power mode. Station 2 acts as the receiving end in this example. The power receiving end always operates in constant power mode in order for the receiving end grid to receive the demanded power despite transmission losses.

A wind turbine is integrated into the system, and the power flow between the grids and the wind farm is observed. The simulation results show that the amount of power transferred from the constant voltage mode end station (i.e., sending end station) is equal to the difference between the amount of power set at the receiving end and the power generated from the wind farm. Given that the transmission loss cannot be neglected, the receiving end stays in constant power mode. In other words,

$$P_{Sending\ end} + P_{wind} + Transmission\ losses = P_{receiving\ end}$$

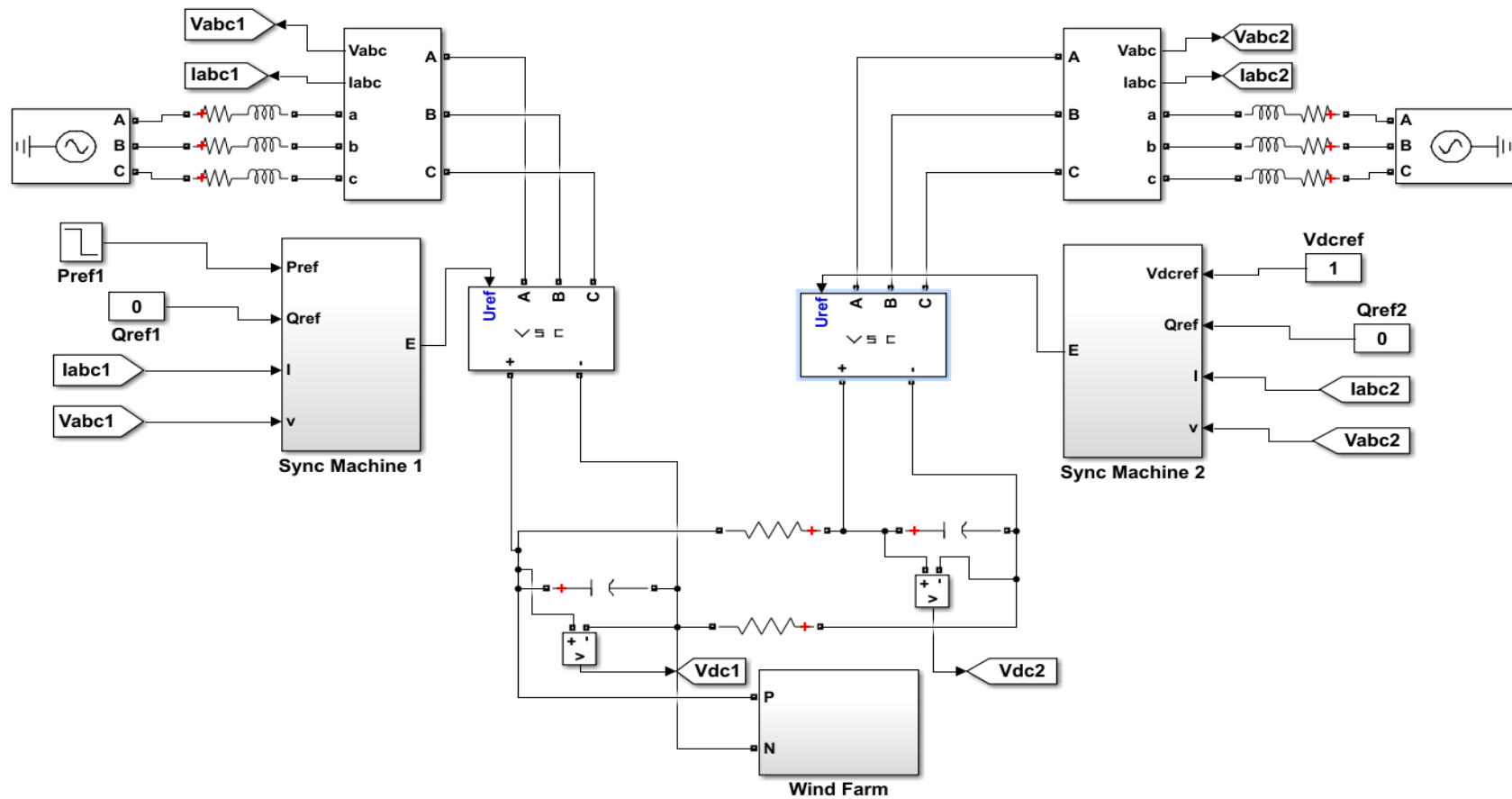


Figure 28: Synchronous Machine Emulation of VSC for the Interconnection of Wind farm Through HVDC Transmission.

3.4 HVDC Power Stabilization using BESS

To stabilize wind power, a large battery energy storage unit is connected to the HVDC link. This battery acts as a reserve storage system that provides or absorbs deficient or surplus power to the HVDC link by using an algorithm that controls the boost converter. This algorithm compares the instantaneous power with the average wind power, and the difference is used to produce a current waveform. The battery current compared with the measured current for the difference in wind power is subsequently used to produce a power reference for the battery conversion system. The current control is developed to ensure that the required power is injected or absorbed into the battery. Figure 29 shows the developed BESS. The load for the boost converter is the HVDC link.

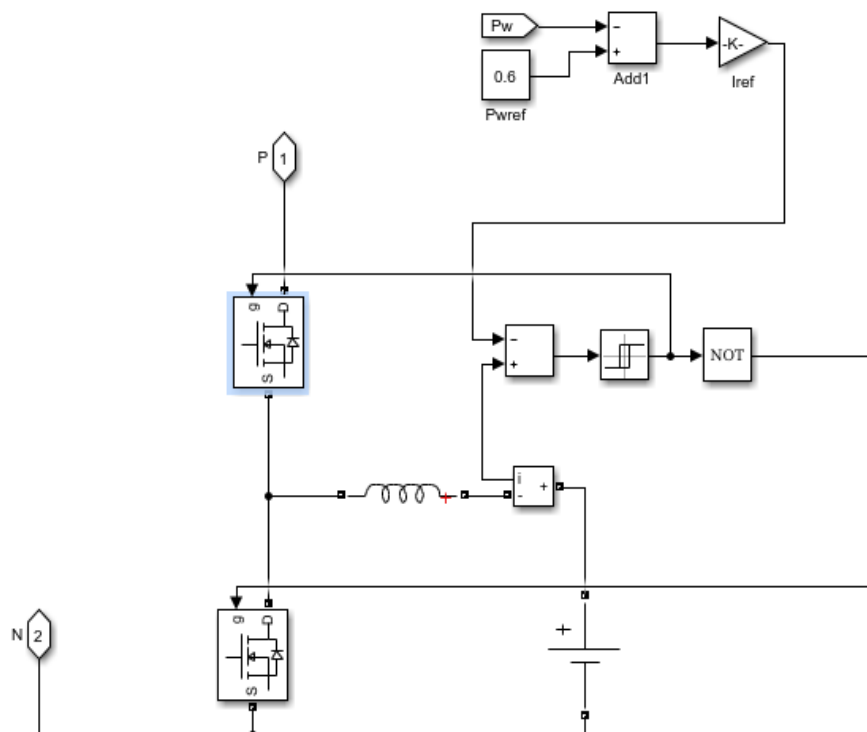


Figure 29: BESS System

Chapter 4: Results and Discussion

4.1 Phase Locked Loop

Figure 30 presents the output of the PLL. The frequency of the grid and the grid phase are both tracked by PLL

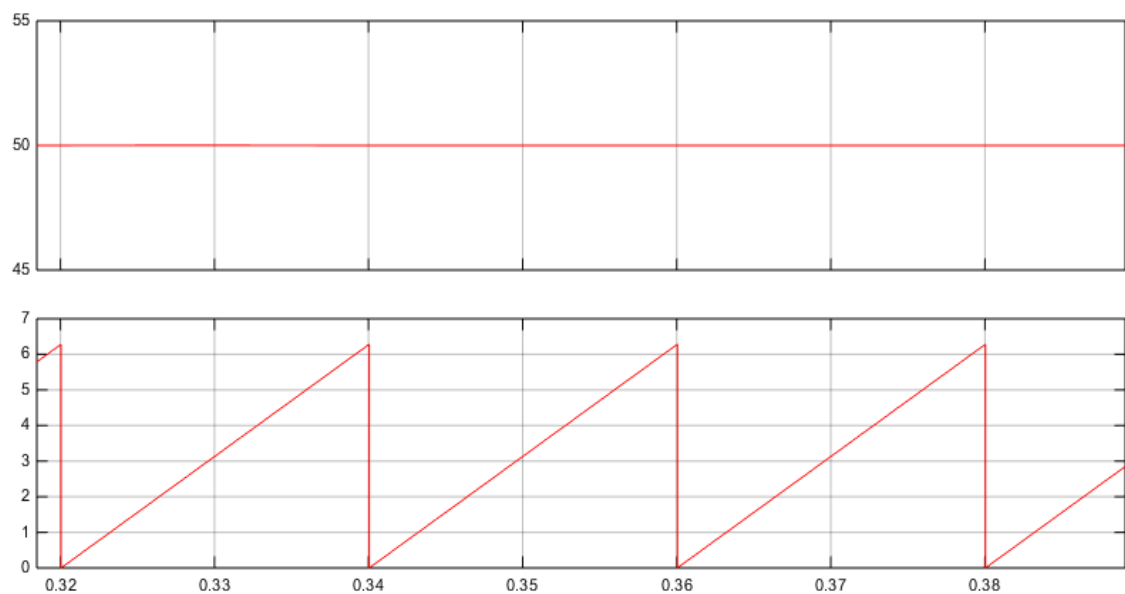


Figure 30: PLL curve

The first figure presents the frequency of the grid (ω , measured in Hz), whereas the second figure presents the grid angle (ωt).

4.2 Case 1: Power Flow between Two Grids Measured by a Synchronverter

Figure 31 shows the real power flow curve between two grids as measured by a synchronverter when a step signal (with initial and final values of 0.9 and 0.3, respectively) is applied at the constant power side with a 2 s time step. The real power curve is tracking to set real power reference curve, and the real power curve at the constant voltage side almost follows the real power curve of the constant power station.

The slight difference in power can be attributed to the transmission losses in the DC link.

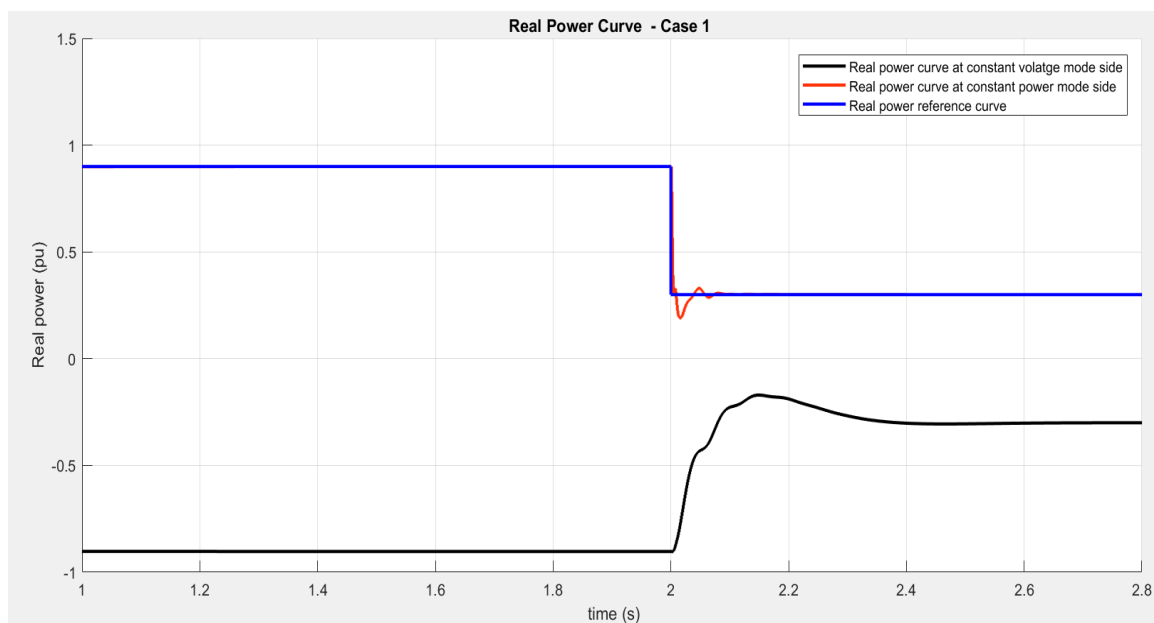


Figure 31: Real Power Graph for Synchronous Machine Emulation of VSC-HVDC

Figure 32 presents the DC link voltage curve at the constant power mode station and the constant voltage mode station of VSC. Both end stations follow the reference voltage curve.

At $t = 2$ s, the input power shifts to 0.3 p.u, thereby producing a slight change in voltage that returns to its initial value between 0.2 s and 0.3 s.

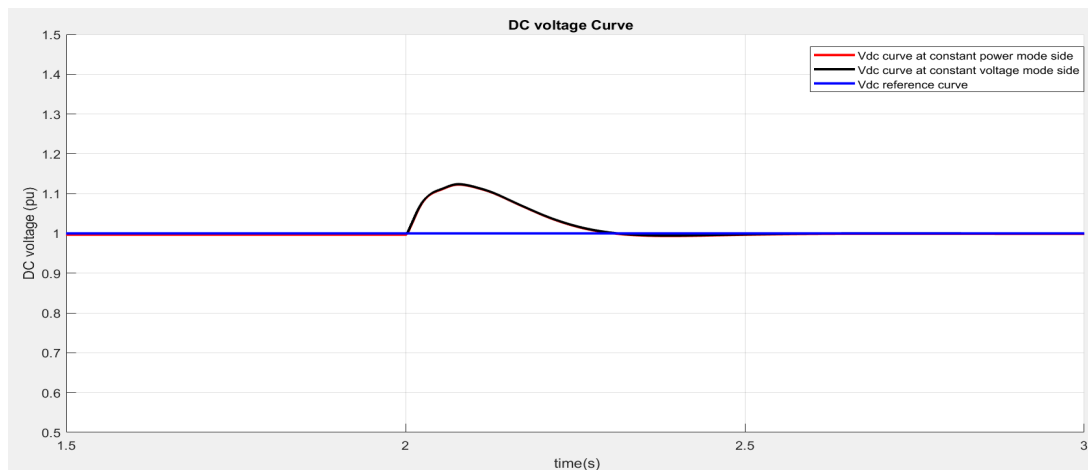


Figure 32: DC Link Voltage Graph at Both Converter Stations

4.3 Case 2: Real Power Graph for the Synchronous Machine Emulation of VSC-HVDC Transmission Interconnected with Wind Farm

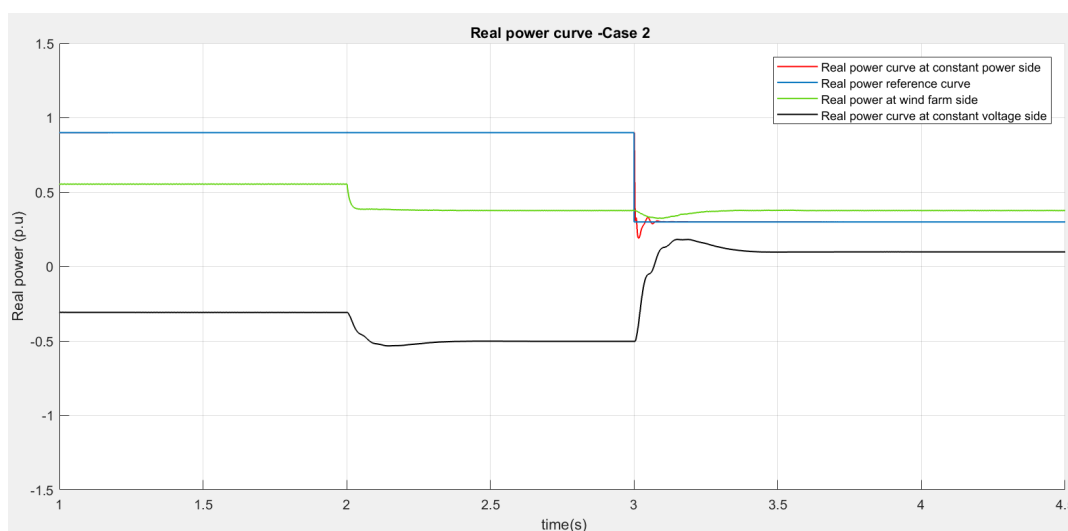


Figure 33: Real Power Graph for the Synchronous Machine Emulation of VSC-HVDC Transmission Interconnected with a Wind Farm

Figure 33 presents the power flow curve for the SM emulation of the VSC-based HVDC transmission system when a wind farm is interconnected to its DC link.

The plot is observed when a step signal of 0.9 p.u to 0.3 p.u at a step time of 3 seconds is fed as the real power reference signal and step signal of 5 to 8 with a step time of 2 seconds applied as the mechanical input to wind farm.

The sum of power drawn from the constant voltage mode side and that generated at the wind farm is approximately equal to the power at the constant power mode side. Therefore, the power at the receiving stations is approximately equal to the sum of power drawn from the sending end station, power generated at the wind farm, and transmission losses.

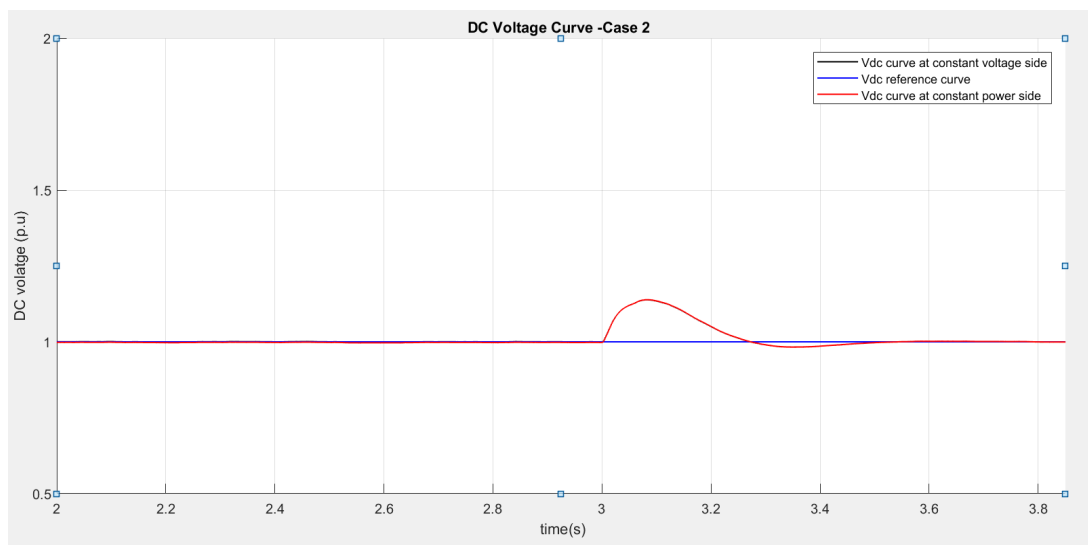


Figure 34: DC link Voltage Graph for the Synchronous Machine Emulation of VSC-HVDC Transmission Interconnected with a Wind Farm.

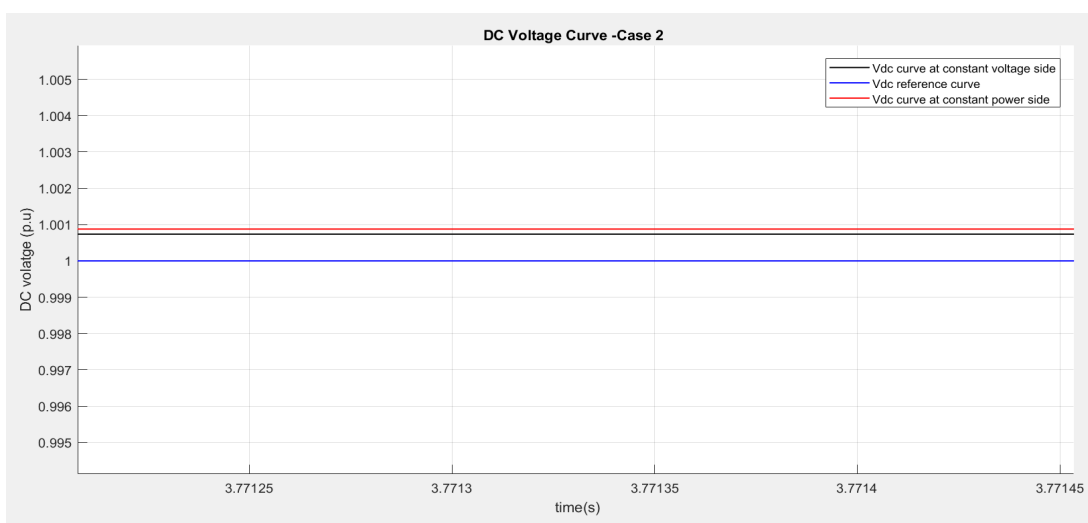


Figure 35: Close view of DC Voltage Curve at Steady State

Figure 34 presents the DC link voltage curve for the SM emulation of a VSC-based HVDC transmission system interconnected with a wind farm, whereas Figure 35 presents a close view of the DC voltage curve at steady state. The DC voltage curves at the constant voltage side and constant power mode closely track the reference curve.

4.4 Case 3: Real Power Graph for the Synchronous Machine Emulation of VSC-HVDC Transmission Interconnected with a Wind farm and BESS.

Figure 36 presents the real power flow for the SM emulation of the VSC-based HVDC transmission interconnected with a wind farm and BESS. The reference real power has a step signal value of 0.9 to 0.3 at a time step of 3 s. The wind farm has a step signal of 5 to 8 at a time step of 2 s.

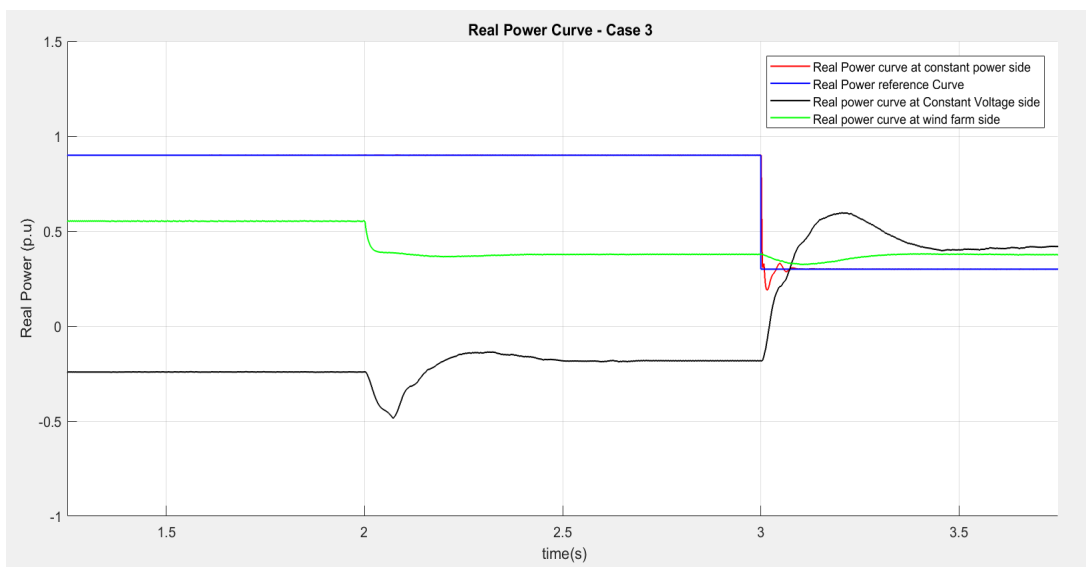


Figure 36: Real Power Graph for Synchronous Machine Emulation of VSC-HVDC Transmission Interconnected with a Wind Farm and BESS.

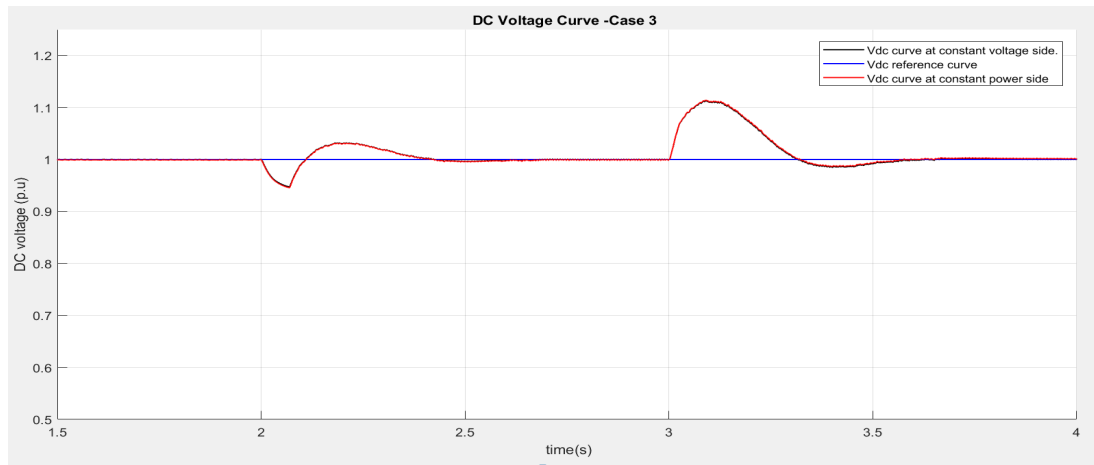


Figure 37: DC Link Voltage Curve for the Synchronous Machine Emulation of VSC-HVDC Transmission Interconnected with a Wind farm and BESS.

Figure 37 demonstrates the DC voltage curve for the SM emulation of the VSC-HVDC system connected with a wind farm and BESS. The slight disturbance observed at $t=2$ s and $t=3$ s and the settling of the DC curve within the acceptable range.

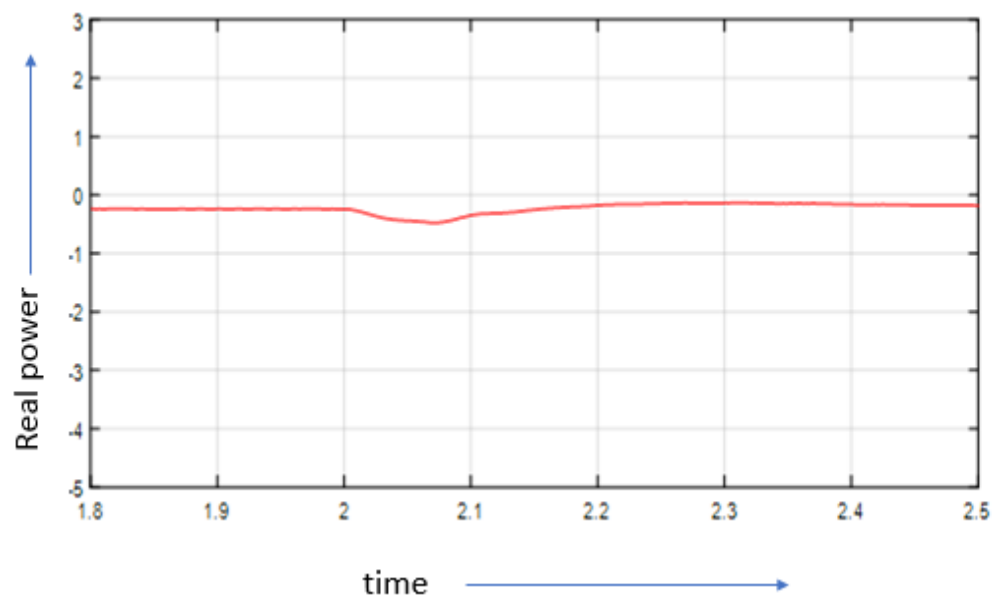


Figure 38: Grid Power Graph with BESS

Figure 38 shows the power curve from station 1 with BESS. At $t=2$ s, wind power starts to fluctuate, whereas the power drawn from the grid remains constant.

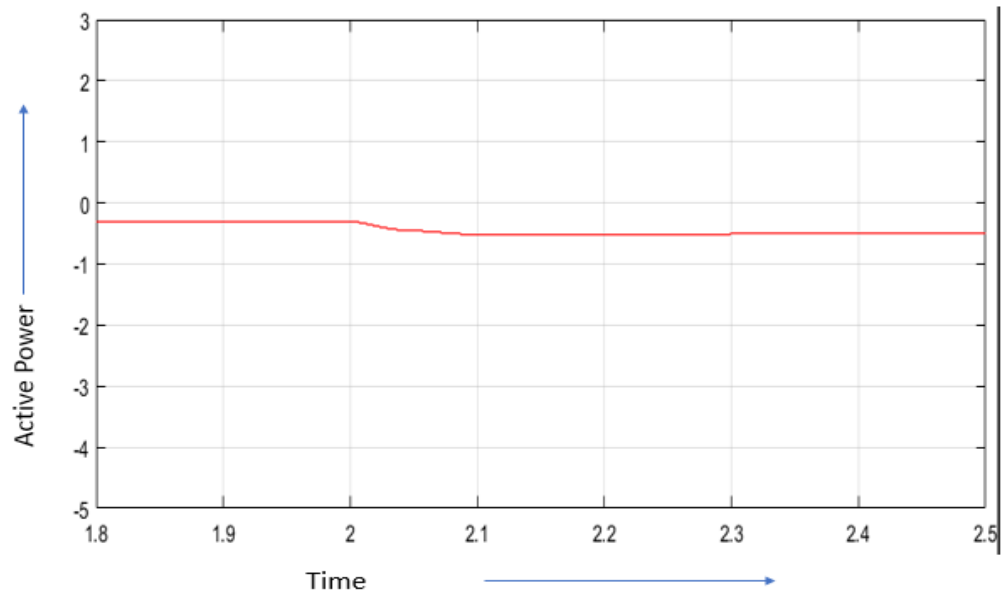


Figure 39: Grid Power Curve without BESS

Figure 39 shows the power curve for station 1 without BESS. At $t = 2$ s, both the wind power and the power drawn from the grid fluctuate.

Chapter 5: Conclusion

This thesis analyzes a synchronverter VSC-based HVDC transmission system and develops an efficient control for transmitting power from one grid to another grid. The power drawn from the grid (stored in the constant voltage mode station) is slightly greater than that received at the receiving end station (operating in constant power mode). The slight difference in power can be ascribed to the transmission losses in the HVDC link.

This thesis develops a model for a VSC-based HVDC transmission system integrated with a wind farm and a method for the auto regulation of power flow between two grids based on the power generated from a wind farm. The simulation results show that the amount of power transferred from the constant voltage mode end station (i.e., sending end station) is equal to the difference between the amount of power set at the receiving end and the power generated from the wind farm.

The power fluctuation in the grid is reduced by the disturbance in wind power with the help of BESS. The disturbance in the power output of the wind farm resulting from the varying nature of wind is compensated by integrating BESS. A reduced power oscillation enhances the stability of the power system. The battery storage system acts as a storage system when surplus power is available and acts as a source that feeds power to the HVDC link when the power supply is deficient. The battery storage system is connected to the DC link of the HVDC by using a bidirectional DC–DC converter.

References

- Abdel-Galil, D. T. K., Abu-Elanien, A. E. B., El-Saadany, D. E. F., & Girgis, D. A. (2007). Protection Coordination Planning with Distributed Generation. Final Report, CETC Varennes, Energy Technology and Programs Sector.
- Alawasa, K. M. (2016). Modeling, Analysis and Simulation of Voltage Sourced Converters- Based High Voltage DC Transmission System (VSC-HVDC). 2(3), 199-213.
- Andersen, B. R. (2006). HVDC Transmission - Opportunities and Challenges. 8th IEEE International Conference on AC and DC Power Transmission (ACDC 2006), 2006, 24–29. <https://doi.org/10.1049/cp:20060006>
- Aouini, R., Elleuch, M., Kilani, K. B., & Marinescu, B. (2016). Synchronverter-Based Emulation and Control of HVDC Transmission. IEEE Transactions on Power Systems, 31(1), 278–286. <https://doi.org/10.1109/TPWRS.2015.2389822>
- De Andrade, L., & De Leao, T. P. (2012). A Brief History of Direct Current in Electrical Power Systems. 2012 Third IEEE History of Electro-Technology Conference (HISTELCON), 1–6. <https://doi.org/10.1109/HISTELCON.2012.6487566>
- De toledo, P. F. (2007). Modeling and Control of a Line-Commutated HVDC Transmission System Interacting with a VSC STATCOM. Phd, Royal Institute of Technology. Stockholm, Sweden.
- Du, C. (2007). The control of VSC-HVDC and its Use For Large Industrial Power Systems. Phd, Chalmers university of Technology. Goteborg, Sweden.
- Durrant, M., Werner, H., & Abbott, K. (2003). Model of a VSC HVDC Terminal Attached to a Weak AC System. Proceedings of 2003 IEEE Conference on Control Applications, 1(1), 178–182. <https://doi.org/10.1109/CCA.2003.1223288>
- Ferreira, R. V., Silva, S. M., Brandao, D. I., & Antunes, H. M. A. (2016). Single-Phase Synchronverter for Residential PV Power Systems. 2016 17th International Conference on Harmonics and Quality of Power (ICHQP), 861–866. <https://doi.org/10.1109/ICHQP.2016.7783378>
- Ganti, V. C., Singh, B., Aggarwal, S. K., & Kandpal, T. C. (2012). DFIG-Based Wind Power Conversion With Grid Power Leveling for Reduced Gusts. IEEE Transactions on Sustainable Energy, 3(1), 12–20. <https://doi.org/10.1109/TSTE.2011.2170862>

- Hammad, A. E., Gagnon, J., & McCallum, D. (1990). Improving the Dynamic Performance of a Complex AC/DC system by HVDC Control Modifications. *IEEE Transactions on Power Delivery*, 5(4), 1934–1943.
<https://doi.org/10.1109/61.103690>
- Harnefors, L., Bongiorno, M., & Lundberg, S. (2007). Input-Admittance Calculation and Shaping for Controlled Voltage-Source Converters. *IEEE Transactions on Industrial Electronics*, 54(6), 3323–3334.
<https://doi.org/10.1109/TIE.2007.904022>
- Hingorani, N. G., & Gyugyi, L. (1999.). *Understanding FACTS*. New York: Wiley IEEE Press.
- Imhof, M. (2015). *Voltage Source Converter Based HVDC - Modelling and Coordinated Control to Enhance Power System Stability*. PhD, ETH Zurich University. Zurich, Switzerland. <https://doi.org/10.3929/ethz-a-010525485>
- Jian Luo, Jianguo Yao, Di Wu, Chuanxin Wen, Shenchun Yang, & Ji Liu. (2011). Application Research on VSC-HVDC in Urban Power Network. 2011 IEEE Power Engineering and Automation Conference, 115–119.
<https://doi.org/10.1109/PEAM.2011.6134921>
- Joos, G., Moran, L., & Ziogas, P. (1991). Performance Analysis of a PWM Inverter VAR compensator. *IEEE Transactions on Power Electronics*, 6(3), 380–391.
<https://doi.org/10.1109/63.85906>
- Jovcic, D., Lamont, L. A., & Xu, L. (2003). VSC Transmission Model for Analytical Studies. 2003 IEEE Power Engineering Society General Meeting (IEEE Cat. No.03CH37491), 3(3), 1737-1742.
<https://doi.org/10.1109/PES.2003.1267418>
- Kazmierkowski, M. P., & Malesani, L. (1998). Current Control Techniques for Three-Phase Voltage-Source PWM Converters: a Survey. *IEEE Transactions on Industrial Electronics*, 45(5), 691–703. <https://doi.org/10.1109/41.720325>
- Konishi, H., Takahashi, C., Kishibe, H., & Sato, H. (2001). A Consideration of Stable Operating Power Limits in VSC-HVDC Systems. Seventh International Conference on AC-DC Power Transmission, 102–106.
<https://doi.org/10.1049/cp:20010526>
- Li, S., Haskey, T.A., Xu, L., (2010). Control of HVDC Light System Using Conventional and Direct Current Vector Control Approaches - *IEEE Transactions on Power Electronics*, 25(12), 3110-3118.
<https://ieeeg.org.ezproxy.uaeu.ac.ae/document/5601788>

- Ooi, B. T., & Wang, X. (1990). Voltage Angle Lock Loop Control of the Boost Type PWM Converter for HVDC Application. *IEEE Transactions on Power Electronics*, 5(2), 229–235. <https://doi.org/10.1109/63.53160>
- Phi-Long Nguyen, Zhong, Q.-C., Blaabjerg, F., & Guerrero, J. M. (2012). Synchronverter-Based Operation of STATCOM to Mimic Synchronous Condensers. 2012 7th IEEE Conference on Industrial Electronics and Applications (ICIEA), 942–947. <https://doi.org/10.1109/ICIEA.2012.6360859>
- Rajan, E., & Amrutha, S. (2017). Synchronverter Based HVDC Transmission. 2017 Innovations in Power and Advanced Computing Technologies (i-PACT), 1–6. <https://doi.org/10.1109/IPACT.2017.8245084>
- Saksvik, O. (2012). HVDC Technology and Smart Grid. 9th IET International Conference on Advances in Power System Control, Operation and Management (APSCOM 2012), 1–6. <https://doi.org/10.1049/cp.2012.2169>
- Svensson, J. (1998). Grid-Connected Voltage Source Converter. Phd, Chalmers University of Technology. Goteborg, Sweden.
- Timbus, A. (2007). Grid Monitoring and Advanced Control of Distributed Power Generation Systems. Phd, Aalborg University. Aalborg, Denmark.
- Younis, T., Ismeil, M., Orabi, M., & Hussain, E. K. (2018). A Single-Phase Self-Synchronized Synchronverter with Bounded Droop Characteristics. 2018 IEEE Applied Power Electronics Conference and Exposition (APEC), 1624–1629. <https://doi.org/10.1109/APEC.2018.8341234>
- Zhang, L., Harnefors, L., & Nee, H. (2010). Power-Synchronization Control of Grid-Connected Voltage-Source Converters. *IEEE Transactions on Power Systems*, 25(2), 809–820. <https://doi.org/10.1109/TPWRS.2009.2032231>
- Zhong, Q., & Weiss, G. (2011). Synchronverters: Inverters That Mimic Synchronous Generators. *IEEE Transactions on Industrial Electronics*, 58(4), 1259–1267. <https://doi.org/10.1109/TIE.2010.2048839>
- Zhou Wei, Chen Jie, & Gong Chunying. (2015). Small Signal Modeling and Analysis of Synchronverters. 2015 IEEE 2nd International Future Energy Electronics Conference (IFEEC), 1–5. <https://doi.org/10.1109/IFEEC.2015.7361434>